

Seeking a coherent explanation of LHC excesses for compressed spectra

Diyar Agin ^{a,1}, Benjamin Fuks ^{b,1}, Mark D. Goodsell ^{c,1}, Taylor Murphy ^{d,1}

¹Laboratoire de Physique Théorique et Hautes Énergies (LPTHE),
UMR 7589, Sorbonne Université & CNRS,
4 place Jussieu, 75252 Paris Cedex 05, France

Accepted 6 November 2024

Abstract The most recent searches by the ATLAS and CMS Collaborations in final states with soft leptons and missing transverse energy show mild excesses predominantly associated with dilepton invariant masses of about 10–20 GeV, which can result from decays of electroweakinos that are heavier than the lightest neutralino by $O(10)$ GeV. On the other hand, these analyses are insensitive to electroweakino mass splittings smaller than about 5 GeV. In previous work, we demonstrated that while recent searches in the monojet channel can exclude some of the smallest $O(1)$ GeV mass splitting configurations for electroweakinos, they also exhibit excesses that can overlap with the soft-lepton excesses in certain models, including a simplified scenario with pure higgsinos. In this work we dive deeper into these excesses, studying the analyses in detail and exploring an array of models that go beyond the simplified scenarios considered by the experimental collaborations. We show that, in the Minimal Supersymmetric Standard Model, the overlapping excesses are not unique to the pure-higgsino limit, instead persisting in realistic parameter space featuring a bino-like lightest supersymmetric particle with some wino admixture. On the other hand, for the Next-to-Minimal Supersymmetric Standard Model with a singlino-like lightest supersymmetric particle and higgsino-like next-to-lightest supersymmetric particle(s), the excess in the two-lepton channel fits rather well with the parameter space predicting the correct relic abundance through freeze out, but the monojet fit is much poorer. Interestingly, the excesses either do not overlap or do not exist at all for two non-supersymmetric models seemingly capable of producing the correct final states.

Keywords Physics beyond the Standard Model · Soft leptons · Monojets · Supersymmetry

1 Introduction

As experimental limits on classic supersymmetric scenarios grow ever tighter, analyses at the Large Hadron Collider (LHC) have increasingly targeted alternative scenarios that are more experimentally challenging, including those with light neutralinos and charginos (hereafter referred to collectively as electroweakinos) whose masses differ by $O(10)$ GeV or less (forming a so-called *compressed spectrum*). Surprisingly, among the many analyses performed during Run 2 of the LHC, both the ATLAS [1, 2] and CMS [3] Collaborations have reported excesses in equivalent searches involving two or more soft leptons, interpreted in terms of simplified supersymmetric scenarios in which the light electroweakinos are composed mostly of higgsinos or the bino and wino. These interpretations are inspired by certain limits of the Minimal Supersymmetric Standard Model (MSSM). The excesses mostly appear in events containing two leptons (2ℓ) with a dilepton invariant mass in the range 10–20 GeV, but very slight excesses are also visible in the ATLAS trilepton (3ℓ) channel. It is moreover at least qualitatively clear, modulo differences in the model interpretations, that the ATLAS and CMS excesses appear in nearly the same regions of simplified higgsino and/or bino-wino MSSM parameter space; this overlap suggests that a model producing a good fit to one soft-lepton analysis may hope to do the same for the other search. These excesses have thus sparked the interest of the phenomenological community, with several papers exploring some consequences for those scenarios in combination with other observables [4–19].

In a previous work [20], we demonstrated that these dilepton excesses are surprisingly compatible with excesses in

^adagin@lpthe.jussieu.fr

^bfuks@lpthe.jussieu.fr

^cgoodsell@lpthe.jussieu.fr

^dmurphy@lpthe.jussieu.fr

monojet events, again appearing in analyses by both the ATLAS [21] and CMS [22] Collaborations. This was achieved by interpreting the monojet signals in terms of the simplified scenario used in both soft-lepton searches in which the lightest supersymmetric particle (LSP) $\tilde{\chi}_1^0$, the next-to-lightest supersymmetric particle (NLSP) $\tilde{\chi}_1^\pm$, and the second-lightest neutralino $\tilde{\chi}_2^0$ constitute a triplet of “pure” higgsinos (we refer to this as the “simplified higgsino” scenario). These findings raised several questions; in particular:

1. Since the simplified higgsino scenario is really a toy model, what happens when we consider *realistic* supersymmetric scenarios, within the MSSM or otherwise?
2. Are there non-supersymmetric models that can explain the excesses?
3. Can any of these models produce a dark matter candidate with suitable relic abundance?

In this work, we begin to address these three questions.

In the ATLAS and CMS compressed electroweakino analyses, the simplified models invariably produce dilepton events through the off-shell decay of a heavy neutralino to the LSP, $\tilde{\chi}_2^0 \rightarrow Z^* + \tilde{\chi}_1^0$, $Z^* \rightarrow \ell^+ \ell^-$. But it is also possible to produce dilepton events through decays of off-shell W bosons through processes such as

$$pp \rightarrow \tilde{\chi}_1^+ \tilde{\chi}_1^-,$$

$$\tilde{\chi}_1^\pm \rightarrow \tilde{\chi}_1^0 + W^{\pm,*}, \quad W^{\pm,*} \rightarrow \ell^\pm \nu. \quad (1)$$

In the simplified higgsino model these contribute a small but non-negligible amount to the signal. On the other hand, in the other scenario considered by the experimental collaborations, in which the LSP is predominantly bino and the NLSP is mostly wino (we refer to this as the “simplified bino-wino” scenario, though as we discuss below, it encompasses two cases), the cross section of the $pp \rightarrow \tilde{\chi}_1^+ \tilde{\chi}_1^-$ process is small enough that the experimental collaborations neglect its contribution in their simulations. Other models with the same pattern of decays could, however, produce such decays with larger rates and these processes could, in principle, provide an explanation of the observed excesses. Furthermore, *two-body* decays could also provide soft dileptons, for example in models with new states that couple directly to leptons. Thus our investigation is aimed, in part, at understanding how the topology of a given 2ℓ signal process affects its ability to fit the excesses observed by the ATLAS and CMS Collaborations. But this has to be done with due regard for the monojet analyses, which veto practically all visible leptons and therefore require any candidate model to produce monojet events through entirely different processes.

Meanwhile, it is generally accepted that models with a higgsino LSP much lighter than 0.5–1.0 TeV predict underabundant dark matter (assuming a standard cosmological history) [23, 24], which by itself motivates non-higgsino interpretations of the compressed LHC excesses. Clearly spurred

(at least in part) by this fact, ATLAS recently performed a study in the phenomenological MSSM (pMSSM) examining limits on their own bino-wino scenarios, comparing the limits from soft-lepton searches to constraints from dark matter searches and elsewhere [25]. But this analysis includes neither their own monojet search¹ nor the CMS analog, in which the excess appears stronger. Thus the results are presented as limits, even though the mild soft-lepton excess can be discerned from their plots.

The starting point for this work is therefore a holistic (re)examination of the bino-wino MSSM scenario. We perform a scan over realistic MSSM parameter space and analyze the resulting points using recasts of all four relevant LHC analyses. Our recasts of the ATLAS 2ℓ and 3ℓ analyses are released alongside this work and documented and validated here for the first time. Further motivated by the dark matter problem, we also identify parameter space within the Next-to-Minimal Supersymmetric Standard Model (NMSSM) that may be suitable for the LHC excesses and perform a similar analysis. We then consider two non-supersymmetric beyond-the-Standard Model (BSM) scenarios that seem like good candidates and interestingly seek to explain the LHC excesses through processes markedly different from their supersymmetric competitors.

This paper is organized as follows. Section 2 describes the soft-lepton (and, briefly, monojet) analyses considered in this work, with particular detail devoted to the various excesses and the validation of our recasts. In Section 3 we begin to interpret the analyses through the lens of BSM physics, starting with a realistic MSSM scenario featuring a bino-wino LSP and decoupled higgsinos. We emphasize the differences between our scenario and the simplified bino-wino model considered by ATLAS, and explore the overlap between the multiple excesses and the parameter space compatible with the observed dark matter relic abundance. We consider the NMSSM in Section 4, demonstrating that light higgsinos and an even lighter singlino can generate a 2ℓ excess compatible with the dark matter relic abundance, but fails to predict enough monojet events. Finally, in Section 5, we show that two seemingly well motivated non-supersymmetric models show either non-overlapping or nonexistent excesses, primarily due to their failure to reproduce the lepton kinematics of the supersymmetric models. Thus the interpretation of these analyses is highly sensitive to the topologies of the signal processes that generate soft lepton pairs. We summarize our findings and suggest future avenues of study in Section 6.

¹We speculate that this omission arises because this analysis was performed by the exotica group, rather than by the supersymmetry group.

2 Discussion of experimental analyses

We begin by reviewing the experimental analyses of interest in this work. We detail the implementation of these analyses in HACKANALYSIS version 2 [26],² which we use as part of a simulation and analysis toolchain to evaluate the compatibility of multiple BSM scenarios with the compressed LHC excesses.

2.1 ATLAS-SUSY-2018-16: Soft dilepton + missing energy

ATLAS-SUSY-2018-16 describes a search by the ATLAS Collaboration for electroweakino pair production in final states with missing transverse momentum and a low-momentum opposite-sign same-flavor (OSSF) lepton pair [1]. This search is motivated by (and indeed targets) supersymmetric models in which the lightest neutralino $\tilde{\chi}_1^0$ is the LSP and is lighter than the next-lightest sparticles (*e.g.*, electroweakinos $\{\tilde{\chi}_1^\pm, \tilde{\chi}_2^0\}$ or sleptons $\tilde{\ell}$) by only $\mathcal{O}(1\text{--}10)$ GeV. Such a spectrum allows a heavier state to produce a soft OSSF lepton pair through its decay to the LSP. A representative electroweakino signal process for this analysis is displayed in Figure 1.

This analysis targets four simplified supersymmetric scenarios inspired by the MSSM. The *higgsino* scenario features a triplet $\{\tilde{\chi}_1^0, \tilde{\chi}_1^\pm, \tilde{\chi}_2^0\}$ of light “pure” higgsinos with equal mass splittings $\Delta m(\tilde{\chi}_2^0, \tilde{\chi}_1^\pm) = \Delta m(\tilde{\chi}_1^\pm, \tilde{\chi}_1^0)$, which resembles the MSSM electroweakino spectrum when $|\mu| \ll |M_1|, |M_2|$. The *bino-wino* scenario, by contrast, is derived from the limit in which $|M_1| < |M_2| \ll |\mu|$ and features a mostly bino LSP lighter than a nearly degenerate pair of mostly wino $\{\tilde{\chi}_1^\pm, \tilde{\chi}_2^0\}$. The ATLAS search targets two bino-wino cases, motivated by the fact that the choice to make the neutralino mixing matrix real forces at least one mass eigenvalue to be negative: in the “wino/bino(+)” scenario, the two lightest neutralinos have masses of the same sign, while in the “wino/bino(−)” scenario, the eigenvalues have opposite sign. We discuss the issue of signed electroweakino mass eigenvalues below, since it has physical implications and turns out to be important for the recasting of this analysis. Whereas in these first two scenarios, electroweakino production is assumed to be driven by *s*-channel *W/Z* boson production, the third *VBF* scenario targets *t*-channel electroweakino production through electroweakino exchanges between weak bosons. Finally, the *slepton* scenario features the pair production of light sleptons, each decaying directly to the LSP and its lepton superpartner.

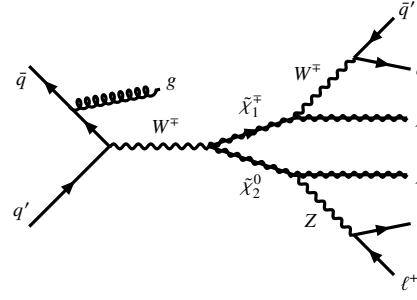


Fig. 1 Representative diagram for a $2\ell + E_T^{\text{miss}}$ signal from light electroweakino pair production. A 3ℓ signal can arise from a leptonically decaying *W* boson.

2.1.1 Selections

This analysis comprises several classes of signal region (SR), each targeting one or more of the BSM scenarios described above. The SRs are categorized as E (electroweakino), VBF, and S (slepton). While we have mentioned the latter two for completeness, only the electroweakino signal regions are re-cast; thus the rest of this discussion is limited to the signal regions labeled by the ATLAS Collaboration as SR-E (with various suffixes in the exclusive channels). The electroweakino search itself contains two channels: the 2ℓ channel is characterized by a pair of OSSF signal leptons, whereas the $1\ell 1T$ channel, which targets the smallest mass splittings, requires one lepton and at least one low- p_T track that can be matched to a lepton of opposite sign.

The preselection requirements are listed in Table 1. As we explore below, the excesses appear in the 2ℓ channels. The leading lepton must have transverse momentum $p_T > 5$ GeV, and the lepton pair must satisfy various requirements on isolation and its invariant mass, depending on the OSSF pair flavor. Missing transverse energy (E_T^{miss}) of at least 120 GeV must be recorded, and at least one jet with $p_T \geq 100$ GeV is required. There are finally isolation requirements on the missing transverse momentum and both the leading jet and any additional jets.

The selection requirements for the electroweakino signal regions are listed in Table 2. As noted above, the electroweakino analysis includes 2ℓ and $1\ell 1T$ channels. The 2ℓ channel moreover contains exclusive signal regions distinguished by requirements on E_T^{miss} and the ratio $E_T^{\text{miss}}/H_T^{\text{lep}}$ of missing transverse energy to the scalar sum of lepton p_T . (The exclusive analysis also reports yields separately for different OSSF lepton pair flavors.) In addition to the E_T^{miss} requirements and additional lepton p_T and isolation cuts, the electroweakino selection imposes requirements on two variables intended to select events with high E_T^{miss} resulting from electroweakino recoils off of initial state radiation (ISR). These variables are

²Available at <https://goodsell.pages.in2p3.fr/hackanalysis>.

Variable	Preselection requirements	
	2ℓ	$1\ell 1T$
Number of leptons (tracks)	2 leptons	1 lepton and ≥ 1 track
Lepton p_T [GeV]	$p_T(\ell_1) > 5$	$p_T(\ell) < 10$
$\Delta R_{\ell\ell}$	$\Delta R_{ee} > 0.30, \Delta R_{\mu\mu} > 0.05, \Delta R_{e\mu} > 0.2$	$0.05 < \Delta R_{\ell, \text{track}} < 1.5$
Lepton (track) charge and flavor	$e^\pm e^\mp$ or $\mu^\pm \mu^\mp$	$e^\pm e^\mp$ or $\mu^\pm \mu^\mp$
Lepton (track) invariant mass [GeV]	$3 < m_{ee} < 60, 1 < m_{\mu\mu} < 60$	$0.5 < m_{\ell, \text{track}} < 5$
J/ψ invariant mass [GeV]	VETO $3 < m_{\ell\ell} < 3.2$	VETO $3 < m_{\ell, \text{track}} < 3.2$
$m_{\tau\tau}$ [GeV]	< 0 or > 160	no requirement
E_T^{miss} [GeV]	> 120	> 120
Number of jets	≥ 1	≥ 1
Number of b -tagged jets	$= 0$	no requirement
Leading jet p_T [GeV]	≥ 100	≥ 100
$\min(\Delta\phi(\text{any jet}, \vec{p}_T^{\text{miss}}))$	> 0.4	> 0.4
$\Delta\phi(j_1, \vec{p}_T^{\text{miss}})$	≥ 2.0	≥ 2.0

Table 1 Preselection requirements applied to all events entering into electroweakino search regions of ATLAS-SUSY-2018-16.

Variable	Electroweakino SR Requirements			
	SR-E-low	SR-E-med	SR-E-high	SR-E- $1\ell 1T$
E_T^{miss} [GeV]	[120, 200]	[120, 200]	> 200	> 200
$E_T^{\text{miss}}/H_T^{\text{lep}}$	< 10	> 10	–	> 30
$\Delta\phi(\text{lep}, \vec{p}_T^{\text{miss}})$	–	–	–	< 1.0
Lepton or track p_T [GeV]	$p_T(\ell_2) > 5 + m_{\ell\ell}/4$	–	$p_T(\ell_2) > \min(10, 2 + m_{\ell\ell}/3)$	$p_T^{\text{track}} < 5$
M_T^S [GeV]	–	< 50	–	–
$m_T(\ell_1)$ [GeV]	[10, 60]	–	< 60	–
R_{ISR}	[0.8, 1.0]	–	$[\max(0.85, 0.98 - 0.02 \times m_{\ell\ell}), 1.0]$	–

Table 2 Selection requirements for the four electroweakino signal regions in ATLAS-SUSY-2018-16.

		SR $m_{\ell\ell}$ bin [GeV]							
		[1,2]	[2,3]	[3,2,5]	[5,10]	[10,20]	[20,30]	[30,40]	[40,60]
SR-E high ee	Observed			1	16	13	8	8	18
	Fitted SM events			0.7 ± 0.4	10.3 ± 2.5	12.1 ± 2.2	10.1 ± 1.7	10.4 ± 1.7	19.3 ± 2.5
SR-E high $\mu\mu$	Observed	5	5	0	9	23	3	5	20
	Fitted SM events	3.4 ± 1.2	3.5 ± 1.3	3.9 ± 1.3	11.0 ± 2.0	17.8 ± 2.7	8.3 ± 1.4	10.1 ± 1.5	19.6 ± 2.3
SR-E med ee	Observed			0	4	11	4		
	Fitted SM events			0.11 ± 0.08	5.1 ± 1.6	7.3 ± 1.9	2.2 ± 0.9		
SR-E med $\mu\mu$	Observed	16	8	6	41	59	21		
	Fitted SM events	14.6 ± 2.9	6.9 ± 2.1	6.2 ± 1.9	34 ± 4	52 ± 6	18.5 ± 3.2		
SR-E low ee	Observed			7	11	16	16	10	9
	Fitted SM events			5.3 ± 1.5	8.6 ± 1.8	16.7 ± 2.5	15.5 ± 2.6	12.9 ± 2.1	18.8 ± 2.2
SR-E low $\mu\mu$	Observed	9	7	7	12	17	18	16	44
	Fitted SM events	15.4 ± 2.4	8.0 ± 1.7	6.5 ± 1.6	11.3 ± 1.9	15.6 ± 2.3	16.7 ± 2.3	15.3 ± 2.0	35.9 ± 3.3

Table 3 Observed event yields and fit results using a control region (CR) + SR background-only fit for the exclusive electroweakino 2ℓ signal regions. Information on CRs, backgrounds, and uncertainties is available in the ATLAS analysis. Bins with upward fluctuations of greater than 1σ over the SM expectation are in **blue**, and those with excesses of 2σ or more are additionally in **bold**; bins with correspondingly large under-fluctuations are in **red** and *italics*.

	SR $m_{\ell, \text{track}}$ bin [GeV]					
	[0.5,1.0]	[1.0,1.5]	[1.5,2.0]	[2.0,3.0]	[3.2,4.0]	[4.0,5.0]
Observed	0	8	8	24	24	16
Fitted SM events	0.5 ± 0.5	6.0 ± 1.9	7.6 ± 2.1	20.7 ± 3.4	24 ± 4	18.1 ± 3.1

Table 4 Observed event yields and fit results using a CR + SR background-only fit for the exclusive electroweakino $1\ell 1T$ regions. Information on CRs, backgrounds, and uncertainties is available in the ATLAS analysis. Only the $m_{\ell, \text{track}} \in [1.0, 1.5]$ GeV bin exhibits (barely) a 1σ upward fluctuation.

Inclusive SR-E	N_{obs}	N_{exp}	$p(s=0)$
$m_{\ell\ell} < 1$ GeV	0	1.0 ± 1.0	0.50
$m_{\ell\ell} < 2$ GeV	46	44 ± 6.8	0.38
$m_{\ell\ell} < 3$ GeV	90	77 ± 12	0.18
$m_{\ell\ell} < 5$ GeV	151	138 ± 18	0.24
$m_{\ell\ell} < 10$ GeV	244	200 ± 19	0.034
$m_{\ell\ell} < 20$ GeV	383	301 ± 23	0.0034
$m_{\ell\ell} < 30$ GeV	453	366 ± 27	0.0065
$m_{\ell\ell} < 40$ GeV	492	420 ± 30	0.027
$m_{\ell\ell} < 60$ GeV	583	520 ± 35	0.063

Table 5 Observed and expected event yields for the inclusive electroweakino regions, defined as the union of the individual electroweakino SRs (both 2ℓ and $1\ell 1T$ channels) for specified upper bounds on $m_{\ell\ell}$. Information on background predictions and uncertainties is available in the ATLAS analysis. A discovery p -value ($p(s=0)$) is computed for each inclusive bin. The four inclusive bins with a p -value smaller than 0.05 are in blue and bold.

defined in terms of hemispheres constructed using the recursive jigsaw reconstruction (RJR) technique [27] orthogonal to the *thrust* axis along which electroweakinos recoil against ISR. They are M_T^S , the transverse mass of the objects in the *supersymmetric-particles hemisphere* S ; and R_{ISR} , the ratio of E_T^{miss} to the transverse momentum of the objects in the *ISR hemisphere*. A requirement on M_T^S is imposed on SR-E-med, while R_{ISR} cuts are placed on SR-E-low and SR-E-high.

In the exclusive analysis, once the cuts in Table 2 are imposed, the dilepton invariant mass ($m_{\ell\ell}$ in the 2ℓ channel and $m_{\ell, \text{track}}$ in the $1\ell 1T$ channel) is binned between 1 GeV and up to 60 GeV for the 2ℓ channel and between 0.5 GeV and 5.0 GeV for the $1\ell 1T$ channel, which again targets BSM spectra with quite strong compression. An inclusive electroweakino analysis is also performed by merging all 2ℓ and $1\ell 1T$ bins below an array of $m_{\ell\ell}$ from 1 GeV to 60 GeV. A “model-independent” discovery p -value is then computed for each bin in the inclusive analysis, and a model-dependent exclusion fit is performed for the exclusive bins.

2.1.2 $m_{\ell\ell}$ distributions: Anatomy of the excess

The expected and observed yields in the exclusive $m_{\ell\ell}$ and $m_{\ell, \text{track}}$ bins are displayed in Table 3 for the 2ℓ channels and in Table 4 for the $1\ell 1T$ channel. The binning of the signal regions according to $m_{\ell\ell}$ allows for better discrimina-

tion between signal and background, and this is therefore the strategy also employed by the equivalent CMS analysis [3]. In principle it also affords a discrimination between different supersymmetric scenarios, because the distribution of the decays is different between the higgsino and wino/bino(+) cases. The excess is noticeable in several 2ℓ bins, mostly with moderate $m_{\ell\ell}$ between 5 GeV and 20 GeV, and the accumulation of excess events in these exclusive bins is reflected in the significant discovery p -values computed by the ATLAS Collaboration for four inclusive signal regions with $m_{\ell\ell} < 40$ GeV, as shown in Table 5. However, it is notable that there are significant *underfluctuations* in several exclusive bins: those of $[3.2, 5]$, $[20, 30]$, $[30, 40]$ GeV for the high- E_T^{miss} $\mu\mu$ region, the $[40, 60]$ GeV bin for the low- E_T^{miss} ee region, and the $[1, 2]$ GeV bin for the low- E_T^{miss} $\mu\mu$ region. These are potentially problematic for any model attempting to explain the excess: because the underfluctuations are so severe, predicting even a few events in these bins would rule out the model. This means that models that predict large numbers of events with $m_{\ell\ell} > 20$ GeV or $m_{\ell\ell} < 5$ GeV are likely excluded, and (as we shall see) means that it is possible to obtain exclusion limits *stronger* than the expected ones for such cases. Hence models that best fit the excess should have an $m_{\ell\ell}$ distribution peaked in the $[5, 10]$ GeV range, and should produce both electron and muon pairs, though seemingly not with identical kinematics.

In the ATLAS (and equivalent CMS) publications, the simplified scenarios considered both produce dilepton events emerging from the production of heavy neutralinos that decay to the LSP via an off-shell Z boson, $\tilde{\chi}_2^0 \rightarrow Z^* + \tilde{\chi}_1^0$. The $m_{\ell\ell}$ distributions of the dileptons produced in this manner are thus invariant under boosts and depend only on the couplings of the neutralinos and the mass differences. The full differential decay rate, ignoring the masses of the leptons, is given by [28, 29]

$$\frac{d\Gamma}{dm_{\ell\ell}} = C m_{\ell\ell} \frac{\{m_{\ell\ell}^4 - m_{\ell\ell}^2[(\Delta m)^2 + M^2] + (M\Delta m)^2\}^{1/2}}{(m_{\ell\ell}^2 - M_Z^2)^2} \times \{-2m_{\ell\ell}^4 + m_{\ell\ell}^2[2M^2 - (\Delta m)^2] + (M\Delta m)^2\}, \quad (2)$$

where $\Delta m = m_{\tilde{\chi}_2^0} - m_{\tilde{\chi}_1^0}$ and $M = m_{\tilde{\chi}_2^0} + m_{\tilde{\chi}_1^0}$ in the basis where the mixing matrices are real: these are *signed eigenvalues*. C represents a normalization constant. Note that there is a sign

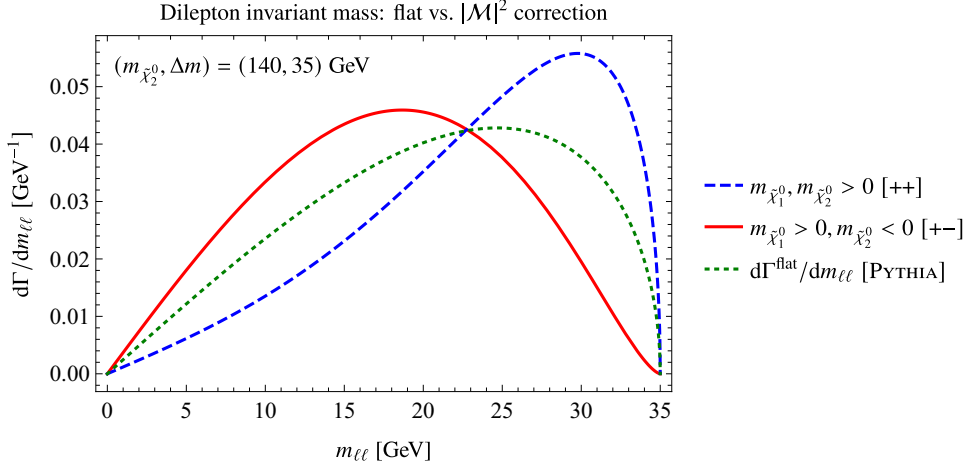


FIG. 2 Dilepton invariant mass distributions for the three cases: both neutralino eigenvalues positive (blue, dashed); opposite-sign eigenvalues (red); flat phase space distribution in which the associated squared matrix element $|\mathcal{M}|^2$ is set to 1 (green, dotted).

error in [28, 29] that we correct in (2).³ Hence if they are of opposite sign, with $m_{\tilde{\chi}_2^0}$ negative as in the ATLAS higgsino and wino/bino(−) scenarios, then Δm and M swap roles; the difference stems from the $2M^2 - (\Delta m)^2$ term.

The expression (2) vanishes at zero and the minimum of $m = |\Delta m|, |M|$. By contrast, in the case of a flat phase space (as used in typical SLHA decay processes in PYTHIA 8, where the contribution from the squared matrix element $|\mathcal{M}|^2$ is unknown and therefore set to unity) the differential decay rate reduces to

$$\frac{d\Gamma^{\text{flat}}}{dm_{\ell\ell}} = C^{\text{flat}} m_{\ell\ell} \times \{m_{\ell\ell}^4 - m_{\ell\ell}^2 [(\Delta m)^2 + M^2] + (M\Delta m)^2\}^{1/2}. \quad (3)$$

We plot these three cases in Figure 2 in a scenario where the NLSP-LSP splitting is $\Delta m = 35$ GeV. While it is clear that a flat distribution does not discriminate between the two signed-eigenvalue scenarios, it turns out that this is not a mere curiosity and the accurate $m_{\ell\ell}$ distributions are vitally important to obtaining a successful reproduction of the experimental results, and therefore also to further interpretations.

In the simplified higgsino scenario (where the eigenvalues have opposite signs), we see that the distribution is flatter and peaked near $\Delta m/2$; whereas in the wino/bino(+) scenario (where they have the same sign) the peak is much closer to the upper endpoint. Hence if we seek to explain an excess by producing events in the range $m_{\ell\ell} \in [5, 20]$ GeV we expect the best fit for the excess for the higgsino case to be around $\Delta m \in [10, 40]$ GeV, and for the wino/bino(+) case to be roughly in the region $\Delta m \in [6, 24]$ GeV. This explains the features in the exclusion plots; therefore, in other models we

can seek to explain the excess (or lack thereof) by plotting their $m_{\ell\ell}$ distributions, as we do through the rest of this work.

2.1.3 Recast and validation

This analysis presents several challenges for both implementation and validation. In the following we describe how this has been achieved in HACKANALYSIS v2, which is now publicly available. This was possible because the ATLAS Collaboration provided substantial supplementary material: a pseudocode for SIMPLEANALYSIS [30]; a PyHF [31] model file for the background model; a set of *signal* patches for the PyHF model file corresponding to a wide variety of higgsino and wino/bino signal points; and cutflows for one parameter point (the higgsino case with $m_{\tilde{\chi}_2^0} = 155$ GeV, $\Delta m = 5$ GeV).

Of the major recasting frameworks, only CHECKMATE [32, 33] has an extant version of this analysis, although seemingly the only validation that was performed was a comparison with the cutflows provided by ATLAS. The main difficulty with recasting this analysis is that it relies on RJR variables (*viz.* Section 2.1) constructed using the RESTFRAMES package [34]; this is a large package that relies on root [35] and many of its functionalities (especially rotations of vectors and minimization methods). Since GAMBIT [36] and MADANALYSIS 5 [37–39] use their own treatments of Lorentz vectors and other features of root, it is not simple to link RESTFRAMES within these platforms. On the other hand, CHECKMATE does use root objects, but in their implementation of this analysis only pseudo-jigsaw variables are used as a proxy to the full use of RESTFRAMES and the package is not linked.

However, HACKANALYSIS was designed to be easily hackable, and so it was possible to create a root-free implementation of RESTFRAMES within HACKANALYSIS. This required the addition of new features in HACKANALYSIS to replace

³In Equation (4) of [29], this comes from (4.21) in [28], but the previous formula (4.18) is correct.

those required from `root`: in particular, minimization routines based on the Nelder-Mead algorithm [40]; and matrix manipulations now provided by the `Eigen` package.⁴ It was possible, however, to adapt the `SIMPLEANALYSIS` helper functions that abstract the interface to `RESTRAMES` such that they could be called like in the pseudocode, and this enables straightforward implementation of any other analyses requiring `RESTRAMES`. The new functions available in `HACKANALYSIS v2` are detailed in the documentation with the code, and the new features are described in a separate manual [26].

Efficiencies for the reconstruction of the signal leptons and tracks were provided in the form of plots, from which it was necessary to scrape the data; these were implemented in the form of functions fit to the scraped data. However, as shown in Table 2, the lowest cut on missing energy in the analysis is $E_T^{\text{miss}} \geq 120$ GeV, where it is known that the trigger efficiency is not high; this requires a reweighting of the events based on scraped data on the ATLAS E_T^{miss} trigger efficiency found in dedicated ATLAS searches. With the efficiencies in hand, it becomes possible to validate the analysis in several ways. We performed a comparison of the cutflows, a comparison of the final yields with those in the signal patchset, and a reproduction of the exclusion plots. We note that the pseudocode provided contains only signal regions (not control regions); using the patchsets, we were able to confirm that the signal contamination in control regions is small (especially compared to the backgrounds) and therefore we only implemented the signal regions in the recast.

One of the striking features of this analysis is its diminutive selection efficiencies: typical cross sections for electroweakino production in the mass range to which this analysis is sensitive are of $\mathcal{O}(1)$ pb, yet producing even three events in the wrong $m_{\ell\ell}$ bin would exclude a model. We thus find typical efficiencies of $\mathcal{O}(10^{-5})$ and for many cases (especially at lower masses and lower Δm) even smaller. Such low efficiencies demand quite large samples in order to achieve acceptable numerical uncertainty and therefore make the simulation of the signals technically challenging.

In the discussion above, we emphasized the importance of the $m_{\ell\ell}$ distributions due to the use of this variable to create signal bins, and because there are severe underfluctuations in certain bins that lead to strong limits upon any model that populates those bins. In the validation we found this to be particularly striking: it is impossible to validate this analysis using a flat phase-space distribution of the three-body decays of neutralinos. To obtain the correct distributions we could, in principle, use `MADSPIN` [41] and `MADWIDTH` [42] if we prepared different event samples for each final state. Instead, we use the decay chain functionality of `MADGRAPH5_AMC@NLO` (MG5_AMC) [43] to compute

the decays including full spin correlations via commands such as

```
MG5_AMC> generate p p > n1 n2, n2 > n1 l+ l-.
```

In this way we force the heavier neutralino to decay to leptons and gain an order of magnitude of efficiency at the detector level, because this branching ratio is less than $\mathcal{O}(10)\%$. On the other hand, for processes involving charginos, since only one lepton can come from their decays, the exact distribution is less important: the reconstructed $m_{\ell\ell}$ will depend more on the mother particle momenta. Hence we model the decays of charginos with a flat phase space in `PYTHIA 8` [44].

Even with such improvement, to obtain uncertainties of $\mathcal{O}(10)\%$ on efficiencies of $\mathcal{O}(10^{-5})$ requires $\mathcal{O}(10^6)$ events. Moreover, for ATLAS' higgsino model we need to separately simulate both $pp \rightarrow \tilde{\chi}_2^0 \tilde{\chi}_1^\pm, \tilde{\chi}_2^\pm \tilde{\chi}_1^0$ and $pp \rightarrow \tilde{\chi}_1^\pm \tilde{\chi}_1^\mp$. Even further, in order to obtain the correct distributions for the missing energy, which depends on the recoil of the electroweakinos from initial-state radiation, we must combine matrix elements including up to two additional partons. After matching the matrix elements in the MLM scheme [45, 46] with a matching scale Q_{cut} fixed⁵ at 40 GeV, we are left with about half of the simulated hard-scattering events. In order to meet these challenges, we leverage the ability to run `HACKANALYSIS` on multiple cores: using a new gridpack mode within `BSMART` [47], we generate for each point in the relevant parameter space a gridpack from MG5_AMC, involving the built-in UFO [48, 49] MSSM implementation [50] and the leading-order set of NNPDF2.3 parton densities [51, 52], and use it to generate one Les Houches Event file [53] for each core, running in parallel. This eliminates one of the major bottlenecks in MG5_AMC (at least for versions prior to 3.5.4) where the simulated events generated for each subprocess are only recombined and reweighted using a single core. Then parton showering is performed within `HACKANALYSIS` using `PYTHIA 8` [44] so that no showered events need be written to disk. In this way, using eight cores, we can analyze 3.2×10^6 events in around four hours per parameter point. We simulate $\mathcal{O}(10^2)$ parameter points for each model and each analysis in this work; the number of points is specified in the discussion of each model.

We book histograms of the $m_{\ell\ell}$ distributions in `HACKANALYSIS` using `YODA` [54]; in Figure 3 we plot the distributions (using the convenient plotting facility of `YODA`) obtained for the process $pp \rightarrow \tilde{\chi}_2^0 + X$, for the higgsino and wino/bino(+) scenarios, for the parameter point $m_{\tilde{\chi}_2^0} = 190$ GeV, $\Delta m = 8$ GeV. We find that the generated distributions match the predictions in Figure 2. On the other hand, a stark difference is visible in Figure 4 for the case of (simplified higgsino) chargino pair production, in which each lepton in the OSSF pair comes from the chargino of matching charge.

⁵A typical value for the matching scale is $Q_{\text{cut}} = m_{\tilde{\chi}}/4$ or the average mass of the produced electroweakinos.

⁴See the webpage <https://gitlab.com/libeigen/eigen>.

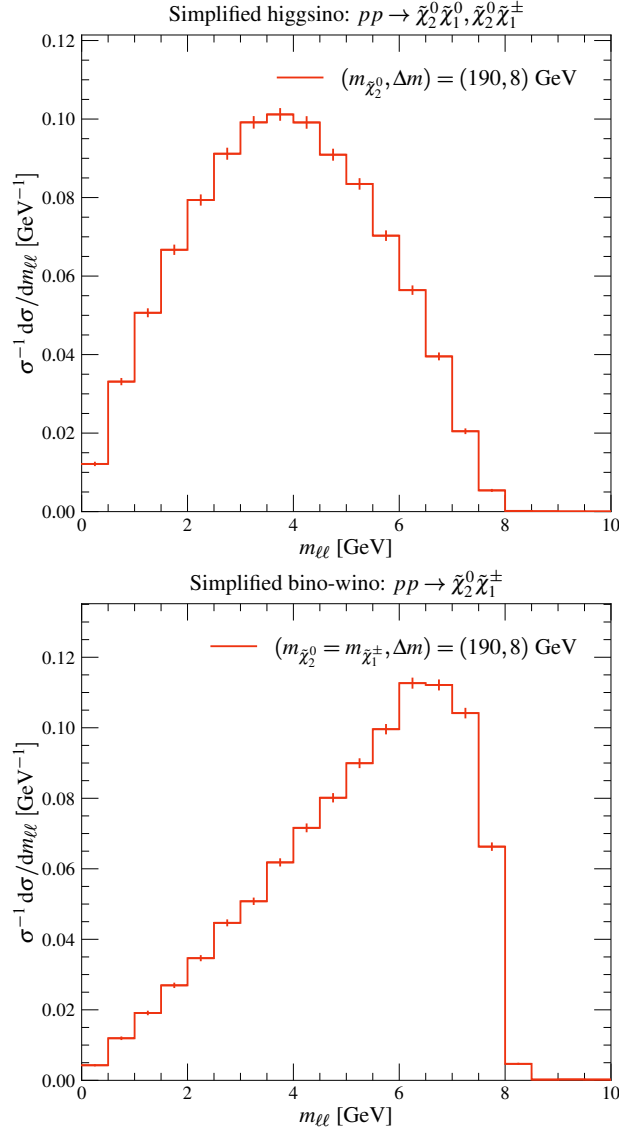


Fig. 3 $m_{\ell\ell}$ distributions for the ATLAS simplified higgsino (left) and bino-wino [wino/bino(+)] (right) cases as found from our simulations for the processes $pp \rightarrow \tilde{\chi}_2^0 \tilde{\chi}_1^\pm$ (and $pp \rightarrow \tilde{\chi}_2^0 \tilde{\chi}_1^0$ for higgsinos) with matrix elements including up to two additional partons.

This distribution is sharply peaked at Δm but has a comparatively long tail for larger $m_{\ell\ell}$. This result suggests that models with decays purely via off-shell W boson(s) will be harder, though not necessarily impossible, to prevent from generating too many events in the larger $m_{\ell\ell}$ bins.

To validate our recast, after comparing the cutflows for the one higgsino point given by ATLAS, we compare signal yields with selected points from the patchset and find excellent agreement. A reliable comparison requires signal cross sections at next-to-leading order in the strong coupling, including next-to-leading logarithmic corrections (NLO + NLL), which we compute for each of our parameter points using RESUMMINO [55, 56]. However, in the patchset it is also evident that the provided signals contain a *statistical uncertainty*: the numbers simulated by ATLAS include un-

certainities of about 5% on the most sensitive signal regions and larger uncertainties on those with smaller number of events. Accounting for this uncertainty makes it possible to validate our recast with exclusion plots for the simplified higgsino and bino-wino cases (specifically wino/bino(+) in the latter case). We simulate 227 simplified higgsino and 368 simplified bino-wino points for this validation. In reproducing ATLAS' exclusion plots, we find that the statistical uncertainty weakens the observed limits by around 20 GeV; it is striking that ATLAS could presumably have improved the reach of their search by simply simulating more signal events. We therefore show a comparison of the expected and observed limits for the simplified higgsino and bino-wino cases in Figure 5 using a flat uncertainty in the PyHF patch of 5%. To be conservative, we further include bands cor-

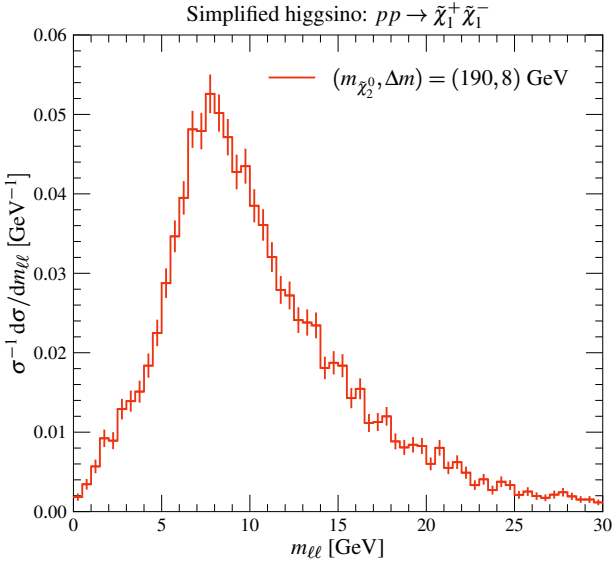


FIG. 4 $m_{\ell\ell}$ distribution for the ATLAS simplified higgsino case as found from our simulations for the chargino pair-production process $pp \rightarrow \tilde{\chi}_1^+ \tilde{\chi}_1^-$, with matrix elements including up to two additional partons.

responding to downward and upward 15% variations of the signal cross sections. Altogether, we find excellent agreement for both models.

2.2 ATLAS-SUSY-2019-09: Three leptons + missing energy

ATLAS-SUSY-2019-09 is described by the ATLAS Collaboration as a search for electroweakino pair production in final states with two or three leptons and missing transverse momentum [2]. More precisely, it consists of a search in the $3\ell + E_T^{\text{miss}}$ channel, which is statistically combined with the results of ATLAS-SUSY-2018-16 in the $2\ell + E_T^{\text{miss}}$ channel, discussed in the previous subsection. Taken together, these searches target pair production of light MSSM electroweakinos with mass splittings ranging from quite small values ($\mathcal{O}(1)$ GeV) to over 100 GeV, depending on the model. To avoid confusion, since we do not perform any statistical combination with our recasts, we clarify here that we use the analysis identifier “ATLAS-SUSY-2019-09” to refer specifically to the 3ℓ channel of the combined analysis. The most important process in the 3ℓ channel is production of the lightest chargino and the second-lightest neutralino, $pp \rightarrow \tilde{\chi}_1^\pm \tilde{\chi}_2^0$. The chargino is again assumed to decay to the LSP and a W boson in all cases, though as before the W may be off shell. Final states with three leptons arise from leptonic decays of the W , so that Figure 1 is easily altered to show a representative 3ℓ signal process. Meanwhile, the assumed decay of $\tilde{\chi}_2^0$ is always to the LSP and an opposite-sign lepton ($\ell \in \{e, \mu\}$) pair, but the SM boson assumed to mediate this decay (and

whether it is on shell) determines the selection criteria and the interpretation of the results. Namely, ATLAS defines the following selections:

- **On-shell WZ** selection: $\tilde{\chi}_2^0 \rightarrow Z\tilde{\chi}_1^0$,
- **Off-shell WZ** selection: $\tilde{\chi}_2^0 \rightarrow Z^*\tilde{\chi}_1^0$,
- **Wh** selection: $\tilde{\chi}_2^0 \rightarrow h\tilde{\chi}_1^0$.

In this work we only make use of the off-shell WZ selection, since that is the only case sensitive to compressed spectra where an excess has been observed. Again we only implement signal regions and not control regions. It should be noted that the on-shell selection has previously been recast in GAMBIT, and we have also implemented that analysis in HACKANALYSIS. The results of the off-shell WZ analysis are interpreted within the same simplified higgsino and wino/bino(\pm) frameworks introduced for ATLAS-SUSY-2018-16.

The preselection requirements for ATLAS-SUSY-2019-09 are listed in Table 6. Exactly three leptons are required, from which set it must be possible to form at least one pair of OSSF leptons that can (naturally) be quite soft. The analysis additionally includes requirements on the minimum and maximum invariant masses $m_{\ell\ell}^{\text{min,max}}$ that can be computed from the OSSF pair(s),⁶ as well as isolation requirements ($\Delta R_{3\ell} = \min \Delta R(\ell_i, \ell_j) \forall \{\ell_i, \ell_j\}$ and $\Delta R_{\text{OSSF}} = \min \Delta R(\ell_i, \ell_j) \forall \text{OSSF} \{\ell_i, \ell_j\}$) and a Z-mass window veto. The analysis further involves low- and high- E_T^{miss} signal regions, with the E_T^{miss} threshold being either $E_T^{\text{miss}} = 50$ GeV or 200 GeV depending on the multiplicity of jets with transverse momentum $p_T(j) > 30$ GeV: the higher E_T^{miss} threshold applies to the SRs with ≥ 1 jet since the electroweakinos have harder recoil in these events. An object-based E_T^{miss} significance, derived from uncertainties on the measurement of individual physics objects [57], is additionally used to control for missed or mismeasured visible objects.

The selection requirements are listed in Table 7, with the SR concatenations employed to conduct an inclusive analysis specified in Table 15 in Appendix A. A fairly large number of exclusive SRs are defined for the off-shell WZ analysis alone. These SRs are principally distinguished by non-overlapping requirements on $m_{\ell\ell}^{\text{min}}$, since this observable has an endpoint at $\Delta m(\tilde{\chi}_2^0, \tilde{\chi}_1^0)$ for the targeted SUSY signals. Additional cuts are imposed on lepton p_T and isolation, as well as on the transverse mass m_T^{mlmin} of the lepton assigned to the W boson and the stransverse mass [58, 59] m_{T2}^{100} of the $(2+1)$ -lepton system (*i.e.*, the combined system comprising the OSSF pair associated with the Z and the lepton assigned to the W^\pm) with a test mass of $m_\chi = 100$ GeV. There are finally cuts on the tripleton invariant mass $m_{3\ell}$ and the ratio $|\vec{p}_T^{\text{miss}}|/E_T^{\text{miss}}$ of the tripleton transverse momentum to the missing transverse energy, the latter of which

⁶This analysis is also performed to identify the lepton most likely associated with the W^\pm decay.

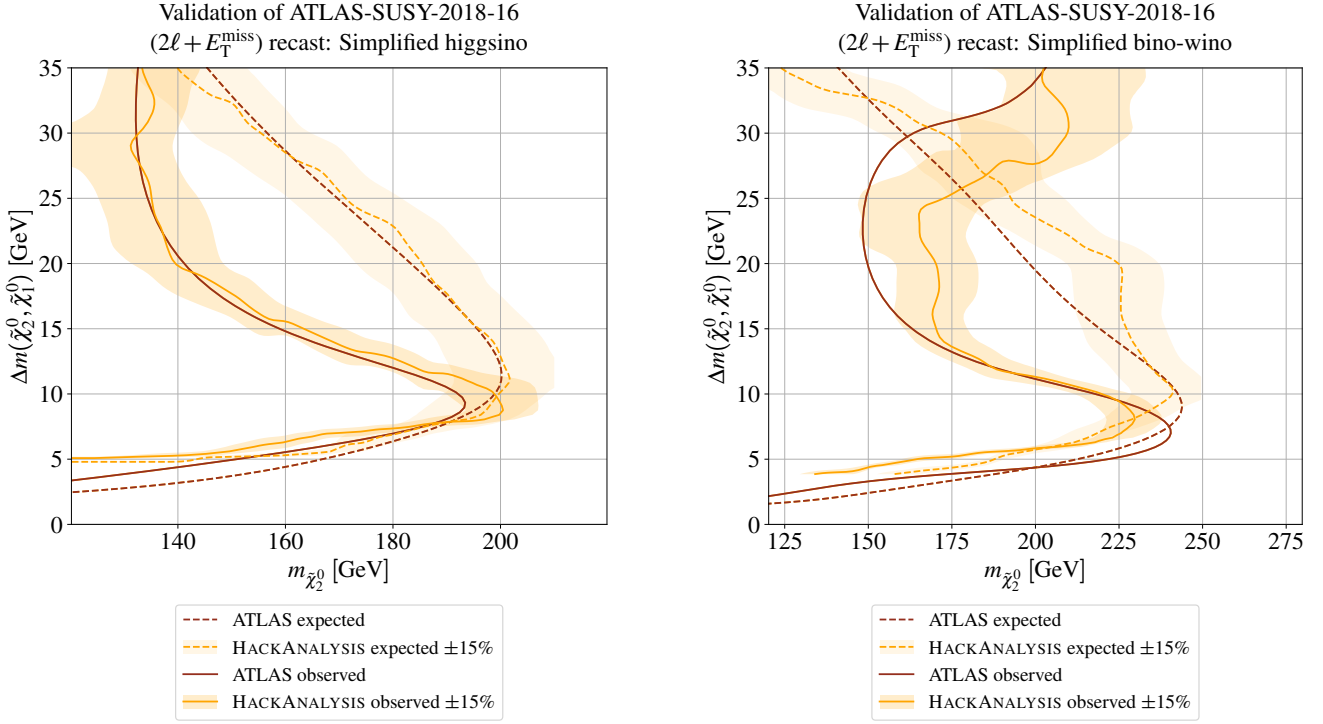


Fig. 5 Comparison of HACKANALYSIS exclusions to official ATLAS results for ATLAS-SUSY-2018-16. Left panel shows exclusions in the simplified higgsino model while right panel refers to the simplified bino-wino scenario. HACKANALYSIS uncertainty bands correspond to 15% variation of the signal strength.

Variable	Preselection requirements			
	$\text{SR}_{\text{low}E_T}^{\text{offFWZ}-0j}$	$\text{SR}_{\text{low}E_T}^{\text{offFWZ}-nj}$	$\text{SR}_{\text{high}E_T}^{\text{offFWZ}-0j}$	$\text{SR}_{\text{high}E_T}^{\text{offFWZ}-nj}$
$n_{\text{lep}}^{\text{baseline}}, n_{\text{lep}}^{\text{signal}}$	$= 3$			
n_{OSSF}	≥ 1			
$m_{\ell\ell}^{\text{max}}$ [GeV]	< 75			
$m_{\ell\ell}^{\text{min}}$ [GeV]	$\in [1, 75]$			
$n_{b\text{-jets}}$	$= 0$			
$\min \Delta R_{3\ell}$	> 0.4			
Resonance veto $m_{\ell\ell}^{\text{min}}$ [GeV]	$\notin [3, 3.2], \notin [9, 12]$		$-$	
Trigger	(multi-)lepton		((multi-)lepton $\parallel E_T^{\text{miss}}$)	
$n_{\text{jets}}^{30 \text{ GeV}}$	$= 0$	≥ 1	$= 0$	≥ 1
E_T^{miss} [GeV]	< 50	< 200	> 50	> 200
E_T^{miss} significance	> 1.5	> 3.0	> 3.0	> 3.0
$p_T^{\ell_1}, p_T^{\ell_2}, p_T^{\ell_3}$ [GeV]	> 10		$> 4.5(3.0)$ for $e(\mu)$	
$ m_{3\ell} - m_Z $ [GeV]	> 20 ($\ell_W = e$ only)		$-$	
$\min \Delta R_{\text{OSSF}}$	$[0.6, 2.4]$ ($\ell_W = e$ only)		$-$	

Table 6 Summary of the preselection criteria applied in the SRs of the off-shell WZ selection in ATLAS-SUSY-2019-09. In rows where only one value is given, it applies to all regions.

Variable	Selection requirements								
	a	b	c	d	e	f1	f2	g1	g2
$m_{\ell\ell}^{\min}$ [GeV]	[1, 12]	[12, 15]	[15, 20]	[20, 30]	[30, 40]	[40, 60]		[60, 75]	
$\text{SR}_{\text{low}E_T}^{\text{offWZ}}$ common									
$m_{\ell\ell}^{\max}$ [GeV]	×	< 60	< 60	< 60	< 60	-	-	-	-
$m_{\text{T}}^{\text{mlmin}}$ [GeV]	×	< 50	< 50	< 50	< 60	< 60	> 90	< 60	> 90
$m_{\text{T}2}^{100}$ [GeV]	×	< 115	< 120	< 130	-	-	-	-	-
$\min \Delta R_{\text{OSF}}$	×	< 1.6	< 1.6	< 1.6	-	-	-	-	-
$p_{\text{T}}^{\ell_1}, p_{\text{T}}^{\ell_2}, p_{\text{T}}^{\ell_3}$ [GeV]	×	> 10	> 10	> 10	> 10	> 15	> 15	> 15	> 15
$\text{SR}_{\text{low}E_T}^{\text{offWZ}} - \emptyset j$									
$ p_{\text{T}}^{\text{lep}} /E_{\text{T}}^{\text{miss}}$	×	< 1.1	< 1.1	< 1.1	< 1.3	< 1.4	< 1.4	< 1.4	< 1.4
$m_{3\ell}$ [GeV]	×	-	-	-	-	> 100	> 100	> 100	> 100
$\text{SR}_{\text{low}E_T}^{\text{offWZ}} - n j$									
$ p_{\text{T}}^{\text{lep}} /E_{\text{T}}^{\text{miss}}$	×	< 1.0	< 1.0	< 1.0	< 1.0	< 1.2	< 1.2	< 1.2	< 1.2
$\text{SR}_{\text{high}E_T}^{\text{offWZ}}$ common									
$m_{\text{T}2}^{100}$ [GeV]	< 112	< 115	< 120	< 130	< 140	< 160	< 160	< 175	< 175
$\text{SR}_{\text{high}E_T}^{\text{offWZ}} - \emptyset j$									
$p_{\text{T}}^{\ell_1}, p_{\text{T}}^{\ell_2}, p_{\text{T}}^{\ell_3}$ [GeV]	×			> 25, > 15, > 10					
$m_{\text{T}}^{\text{mlmin}}$ [GeV]	×	< 50	< 50	< 60	< 60	< 70	> 90	< 70	> 90
$\text{SR}_{\text{high}E_T}^{\text{offWZ}} - n j$									
f g									
$p_{\text{T}}^{\ell_1}, p_{\text{T}}^{\ell_2}, p_{\text{T}}^{\ell_3}$ [GeV]				> 4.5 (3.0) for $e (\mu)$					
$ p_{\text{T}}^{\text{lep}} /E_{\text{T}}^{\text{miss}}$	< 0.2	< 0.2	< 0.3	< 0.3	< 0.3	< 1.0		< 1.0	

Table 7 Summary of the selection criteria for exclusive SRs for the off-shell WZ selection in ATLAS-SUSY-2019-09. SRs are given by the combination(s) of preselection cuts in Table 6 with those listed in this table ($\text{SR}_{\text{low}E_T}^{\text{offWZ}} - \emptyset j$ a, etc.). The symbol \times indicates regions not considered.

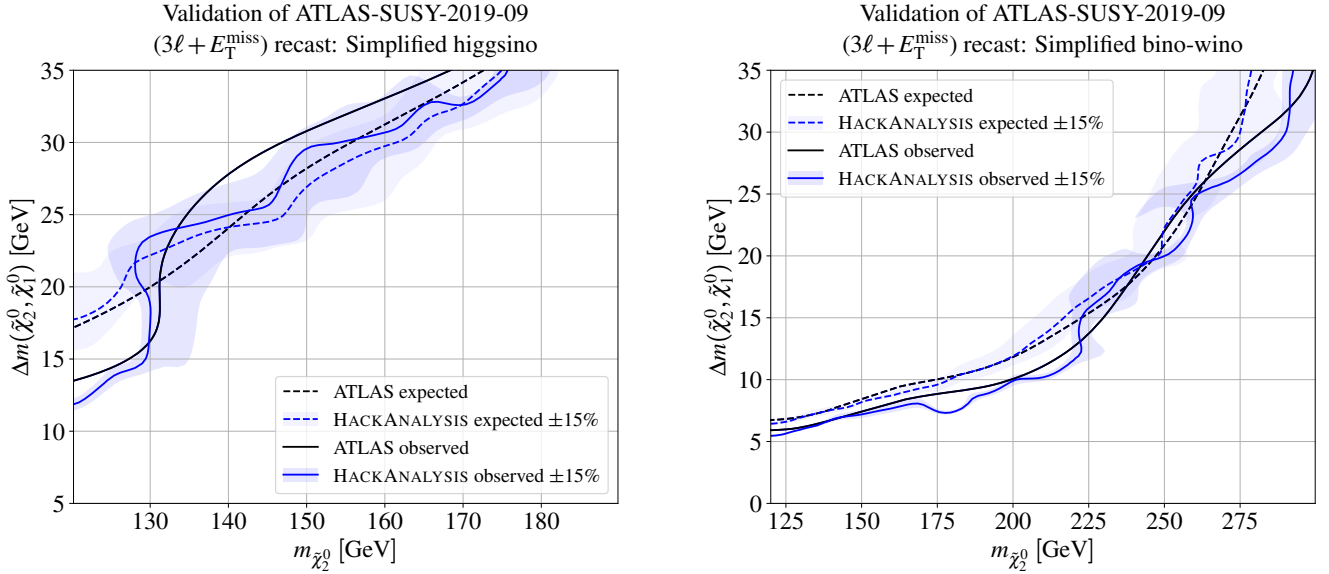


Fig. 6 Comparison of HACKANALYSIS exclusions to official ATLAS results for ATLAS-SUSY-2019-09. Left panel shows exclusions in the simplified higgsino model while right panel refers to the simplified bino-wino scenario. HACKANALYSIS uncertainty bands correspond to 15% variation of the signal strength.

targets events with E_T^{miss} resulting from massive $\tilde{\chi}_1^0$ escaping detection. The ATLAS Collaboration reports expected and observed yields in the 31 exclusive signal regions (which we do not reproduce here for want of space) and in the 17 inclusive signal regions constructed according to Table 15. The inclusive yields are shown in our Table 16, in Appendix A, along with the discovery p -value computed by ATLAS for each signal region.

As stated above, the on-shell and off-shell selections (but not the Wh selection) have now been implemented in HACKANALYSIS; here we discuss only the recast and validation of the off-shell version, since that is the one used in the present work. For this purpose, the ATLAS Collaboration provided a pseudocode, efficiencies for the reconstruction of the leptons in the form of plots (which could be scraped), cutflows, and a PyHF background model. Yet the particulars of the off-shell selection nevertheless present an interesting challenge to recast: for instance, only one class of signal regions contains a straightforward cut on minimum missing transverse energy of 200 GeV; as mentioned above, the others either require $E_T^{\text{miss}} > 50$ GeV or in fact have *upper* bounds of 50 or 200 GeV. The additional multilepton triggers in those signal regions compensate for the known inefficiency of the E_T^{miss} trigger below 200 GeV. In addition, the object-based E_T^{miss} significance, which is not entirely trivial to implement in a recast, is used only in the off-shell selection. This is perhaps why only the on-shell WZ analysis has been implemented in GAMBIT, since it does not rely on this quantity.

In order to model the lepton trigger efficiencies, data from dedicated ATLAS studies [60, 61] were used; the trigger efficiencies for events featuring dielectrons and single, double and triple muons can be found, and from these the probability that a given event will activate one of the triggers can be inferred by checking each case in turn. For the E_T^{miss} significance, defined and studied in [57], it is possible to compute an uncertainty associated to each physics object (jets and leptons in this case, but in principle also photons) using the data in that reference. The data there give the uncertainty on the resolution of the momenta for any such object along its direction of motion, σ_{\parallel} , and perpendicular to it, σ_{\perp} , in the plane perpendicular to the beam axis. The aim is to determine a covariance matrix of uncertainties, given by

$$\mathbf{V}_{xy} \equiv \begin{pmatrix} \sigma_{xx}^2 & \sigma_{xy}^2 \\ \sigma_{xy}^2 & \sigma_{yy}^2 \end{pmatrix} = R^{-1}(\phi) \begin{pmatrix} \sigma_{\perp}^2 & 0 \\ 0 & \sigma_{\parallel}^2 \end{pmatrix} R(\phi), \quad (4)$$

introducing a rotation matrix $R(\phi)$. The sum of all of these matrices for each object can then be added to a component from the “soft term,” which we take to be diagonal with magnitude $(8.9 \text{ GeV})^2$. The E_T^{miss} significance $\mathcal{S}(E_T^{\text{miss}})$ is then given as

$$[\mathcal{S}(E_T^{\text{miss}})]^2 \equiv \mathbf{p}_{\perp}^{\text{miss}} \cdot (\mathbf{V}_{xy}^{\text{total}})^{-1} \cdot \mathbf{p}_{\perp}^{\text{miss}}. \quad (5)$$

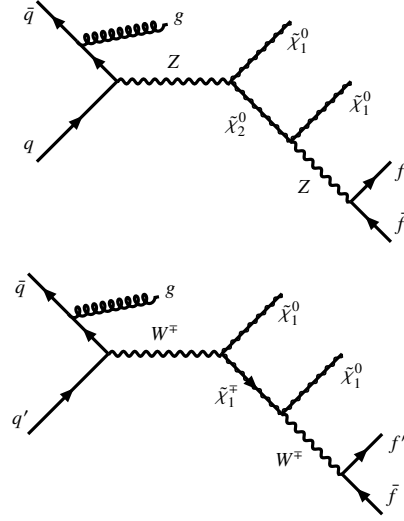


FIG. 7 Representative diagrams for monojet signals originating from light electroweakino pair production. The fermions f, f' must be soft.

In HACKANALYSIS we evaluate this in the analysis from the relevant reconstructed objects. We use uncertainties on each class of object scraped from data in [57] and parameterized as a function of transverse momentum.

To validate our recast of the off-shell WZ selection, we again compare with both the simplified higgsino and wino/bino(+) scenarios using the same simulated events as for the 2ℓ analysis, plus events from additional parameter points where necessary (while the neutralino decays are biased, the chargino decays are not forced to be hadronic for $\tilde{\chi}_2^0 \tilde{\chi}_1^{\pm}$ events in order to make this possible). We simulate 239 simplified higgsino and 475 simplified bino-wino points for this validation. The comparison of exclusion plots for these scenarios is shown in Figure 6. The signals provided for ATLAS-SUSY-2019-09 do not carry a (non-negligible) statistical uncertainty like those in ATLAS-SUSY-2018-16; the only uncertainty estimate in Figure 6 therefore comes from the 15% variation of our own signal strengths. In both model scenarios we find very good agreement with the official results.

2.3 Monojet searches: ATLAS-EXOT-2018-06 and CMS-EXO-20-004

The monojet searches by ATLAS [21] and CMS [22] were previously recast in MADANALYSIS 5 [62, 63]; for statistical information, single-bin data for the ATLAS search must be used (since no statistical information was provided) while CMS provided simplified-likelihood yields and a covariance matrix. These searches are interpreted within different model frameworks but can be reinterpreted for electroweakino pair production followed by decays to the LSP and soft Standard Model fermions, as exemplified in Figure 7. In principle,

E_T^{miss} [GeV]	Background	Observed	χ [σ]
[200, 250]	1783000 ± 26000	1791624	0.3
[250, 300]	753000 ± 9000	752328	-0.1
[300, 350]	314000 ± 3500	313912	-0.0
[350, 400]	140100 ± 1600	141036	0.6
[400, 500]	101600 ± 1200	102888	1.1
[500, 600]	29200 ± 400	29458	0.6
[600, 700]	10000 ± 180	10203	1.1
[700, 800]	3870 ± 80	3986	1.4
[800, 900]	1640 ± 40	1663	0.6
[900, 1000]	754 ± 20	738	-0.8
[1000, 1100]	359 \pm 10	413	5.4
[1100, 1200]	182 ± 6	187	0.8
[1200, ∞]	218 ± 9	207	-1.2

Table 8 Number of expected and observed events by signal bin for the ATLAS monojet search. For each bin we give the χ -value defined as $(\text{observed} - \text{background})/(\text{background uncertainty})$.

these analyses’ rejection of leptons and (additional) jets with p_T of more than a few GeV makes them sensitive to very small electroweakino mass splittings and thus complementary to the soft-lepton searches discussed above. In previous work [20], however, we discussed the presence of excesses in both of those searches; in the ATLAS analysis these occur for $E_T^{\text{miss}} > 400$ GeV, with a 5σ local excess in the bin with $E_T^{\text{miss}} \in [1000, 1100]$ GeV. In an attempt to compare the ATLAS and CMS excesses, we show the equivalent information for the two analyses in Tables 8 and 9. Intriguingly, the CMS analysis shows many excesses in the 2018 dataset with apparent local significances approaching five standard deviations; the CMS bin closest to the ATLAS excess bin, with $E_T^{\text{miss}} \in [1020, 1090]$ GeV, has a local excess of 3.88σ . But the 2016 dataset also contains excesses of up to 3σ in bins with E_T^{miss} ranging from 550 GeV to 740 GeV. Altogether, while it is relatively easy to infer the existence of some excess from both tables, it is not so straightforward to map the ATLAS excess onto the CMS analysis. Further investigation is probably warranted.

A further comment about the CMS monojet excesses is also in order. In Figure 4 of [22], plots are presented showing the number of events observed and the predicted number of background events prior to and post fitting to all the background and signal regions, and while mild excesses can be seen, they do not correspond to the values that are given in Table 9; this can cause some confusion. The values presented here, which we took from the HEPDATA entry, correspond to values computed by CMS to be used as inputs for the simplified likelihood computation, which had a different fitting procedure involving just the control regions, as it should be when we have integrated them out. It is not surprising that the excesses are diminished after a fit to all regions, but perhaps more surprising is that the pre-fit results shown by CMS have a different pattern of deviations: the difference comes from the behavior of the control regions.

For the purposes of this work, the recasts have been adapted into HACKANALYSIS so that the same signal events could be processed through all four analyses at the same time (where appropriate; *i.e.*, when no bias is imposed on the signal generation); this also obviates the need for a DELPHES [64] simulation. The validation for CMS-EXO-20-004 was performed using the same models and cutflows as the MADANALYSIS 5 validation [22], obtaining agreement on the cutflows up to the final cut within 3%, and within 10% or 2σ statistical uncertainty on all missing-energy bins. Validation material for these recasts will be provided elsewhere.

3 Overlapping excesses in a realistic MSSM with bino-wino LSP

In previous work [20], we demonstrated that the mild excesses in the soft-dilepton and monojet channels overlap to some degree for scenarios featuring compressed “pure” higgsinos. Since one aim of this work is to understand if the higgsino scenario is optimal or even unique with respect to these excesses, we use the recasts described in the previous section to reinterpret the analyses for a suite of models. We first consider a limit of the MSSM in which the higgsinos are decoupled, which is not only orthogonal to the light-higgsino scenario (both simplified and realistic) but also distinct from the bino-wino scenario considered in ATLAS-SUSY-2018-16.

One reason to explore the case of a bino-like LSP is the suitability of the bino as a light (sub-TeV) dark matter candidate: unlike higgsinos, which annihilate too quickly and yield underabundant dark matter unless the LSP attains roughly 1 TeV in mass, scenarios with heavy higgsinos can predict much slower electroweakino (co)annihilation. This is certainly one motivation behind ATLAS’ choice to target bino-wino (N)LSP scenarios in their soft-lepton analyses. On the other hand, ATLAS makes some artificial choices in the generation of the parameter cards for the simplified bino-wino signals in the soft-lepton analyses (we elaborate on this below). It is therefore worthwhile, and complementary to our work in [20], to define a “realistic” bino-wino parameter space and interpret the various analyses within this framework. Our scenario most closely resembles the ATLAS wino/bino(+) model but differs in a few subtle but important ways; we discuss these differences further below using a pair of benchmark points.

We are interested in a scenario where the light electroweakinos are composed entirely of gauginos; *i.e.*, the higgsinos are decoupled. In the limit $M_1 < M_2 \ll \mu$, which guarantees a bino-like LSP, the light electroweakino masses

E_T^{miss} [GeV]	2016			2017			2018		
	Background	Observed	χ [σ]	Background	Observed	χ [σ]	Background	Observed	χ [σ]
[250, 280]	135004.86 \pm 3514.65	136865	0.5	169737.77 \pm 3706.95	176171	1.74	178470.12 \pm 3615.00	191829	3.70
[280, 310]	73681.17 \pm 1904.73	74340	0.3	93266.64 \pm 1975.68	96067	1.42	97428.42 \pm 1896.81	104522	3.74
[310, 340]	42448.18 \pm 822.14	42540	0.1	54175.54 \pm 1117.22	54789	0.55	55592.19 \pm 1059.45	59398	3.59
[340, 370]	25541.24 \pm 513.41	25316	-0.4	32232.17 \pm 665.78	32767	0.80	33037.13 \pm 618.12	35833	4.52
[370, 400]	15454.11 \pm 315.39	15653	0.6	19798.25 \pm 413.29	20209	0.99	20714.72 \pm 391.42	21854	2.91
[400, 430]	10162.68 \pm 195.49	10092	-0.4	12816.66 \pm 266.21	12910	0.35	13209.01 \pm 250.28	14266	4.22
[430, 470]	8473.07 \pm 168.65	8298	-1.0	10626.92 \pm 217.70	10653	0.12	10991.22 \pm 213.74	11730	3.46
[470, 510]	4853.26 \pm 106.33	4906	0.5	6407.87 \pm 133.23	6487	0.59	7836.98 \pm 152.03	8639	5.28
[510, 550]	2960.10 \pm 67.10	2987	0.4	3903.66 \pm 84.55	3955	0.61	4914.64 \pm 101.04	5406	4.86
[550, 590]	1906.69 \pm 50.32	2032	2.5	2519.86 \pm 58.43	2587	1.15	3065.69 \pm 66.79	3285	3.28
[590, 640]	1498.36 \pm 39.65	1514	0.4	1929.79 \pm 45.84	1957	0.59	2428.39 \pm 55.08	2671	4.40
[640, 690]	839.22 \pm 26.10	926	3.3	1181.81 \pm 30.83	1151	-1.00	1441.83 \pm 35.64	1613	4.80
[690, 740]	523.39 \pm 17.78	557	1.9	713.79 \pm 21.29	721	0.34	903.52 \pm 24.56	965	2.50
[740, 790]	322.84 \pm 13.17	316	-0.5	456.23 \pm 16.28	455	-0.08	603.29 \pm 18.99	640	1.93
[790, 840]	221.07 \pm 10.19	233	1.2	294.63 \pm 11.86	298	0.28	385.55 \pm 14.01	424	2.74
[840, 900]	167.22 \pm 9.56	172	0.5	231.17 \pm 10.18	244	1.26	271.75 \pm 10.78	319	4.38
[900, 960]	106.22 \pm 6.98	101	-0.7	146.41 \pm 7.44	146	-0.05	176.46 \pm 8.49	191	1.71
[960, 1020]	87.38 \pm 6.92	65	-3.2	87.26 \pm 5.39	89	0.32	117.78 \pm 6.52	117	-0.12
[1020, 1090]	52.37 \pm 4.72	46	-1.4	69.26 \pm 4.73	65	-0.90	75.92 \pm 5.18	96	3.88
[1090, 1160]	24.70 \pm 3.15	26	0.4	32.27 \pm 3.23	39	2.08	48.50 \pm 3.76	55	1.73
[1160, 1250]	25.23 \pm 3.05	31	1.9	30.65 \pm 3.12	35	1.39	35.88 \pm 3.39	43	2.10
[1250, ∞]	26.61 \pm 3.10	29	0.8	37.35 \pm 3.33	40	0.80	53.36 \pm 4.06	70	4.10

Table 9 Number of expected and observed events by signal bin and year for the CMS monojet search. For each bin we give the χ -value defined as (observed-background)/(background uncertainty).

are given approximately by [65]

$$\begin{aligned}
m_{\tilde{\chi}_1^0} &\simeq M_1 + (m_Z \sin \theta_w)^2 \frac{M_1 + \mu \sin 2\beta}{M_1^2 - \mu^2}, \\
m_{\tilde{\chi}_1^\pm} &\simeq M_2 + m_W^2 \frac{M_2 + \mu \sin 2\beta}{M_2^2 - \mu^2}, \\
\text{and } m_{\tilde{\chi}_2^0} &\simeq M_2 + (m_Z \cos \theta_w)^2 \frac{M_2 + \mu \sin 2\beta}{M_2^2 - \mu^2}
\end{aligned} \quad (6)$$

with θ_w denoting the weak mixing angle, m_Z and m_W the masses of the Z and W bosons, and $\tan \beta = v_u v_d^{-1}$ the ratio of the Higgs vacuum expectation values. For NLSP-LSP mass splittings $\Delta m(\tilde{\chi}_2^0, \tilde{\chi}_1^0)$ in the vicinity of 20 GeV, the bino-like $\tilde{\chi}_1^0$ is a viable dark matter candidate with a relic abundance close to the value $\Omega h^2 = 0.12 \pm 0.001$ reported by the Planck Collaboration assuming a standard cosmological history [66]. In this parameter space, the correct relic abundance is achieved principally via (co)annihilations of the other light electroweakinos, notably $\tilde{\chi}_2^0 \tilde{\chi}_1^- \rightarrow \bar{u}d$, $\tilde{\chi}_2^0 \tilde{\chi}_2^0 \rightarrow W^+W^-$, and $\tilde{\chi}_1^+ \tilde{\chi}_1^- \rightarrow W^+W^-, ZZ$.

3.1 Parameter space scan and event generation

To explore this parameter space and produce the various inputs needed for event generation, we use BSMART to steer a random scan of the bino-wino plane (M_1, M_2). The variable

inputs for this scan are simply

$$M_1, M_2 \in [125, 325] \text{ GeV}, \quad (7)$$

and the other relevant parameters are fixed as follows:

$$\begin{aligned}
\mu &= 2 \text{ TeV and } \tan \beta = 25, \\
M_A^2 &= 2.5 \times 10^7 \text{ GeV}^2, \\
M_{\tilde{q}}^2 = M_{\tilde{u}, \tilde{d}}^2 &= (8.25 \times 10^8, 8.25 \times 10^8, 1.25 \times 10^7) \text{ GeV}^2, \\
A_t &= 3.5 \text{ TeV}, \\
M_{\tilde{\ell}}^2 = M_{\tilde{e}}^2 &= (4.25 \times 10^8, 4.25 \times 10^8, 4.25 \times 10^6) \text{ GeV}^2.
\end{aligned} \quad (8)$$

Here $M_{\tilde{f}}^2$ represent the non-negligible flavor-diagonal elements of the softly SUSY-breaking scalar mass matrices of the sfermions \tilde{f} , and A_t stands for the SUSY-breaking trilinear top squark coupling. We emphasize the significant decoupling of the first- and second-generation sfermions. The fixed values guarantee decoupled higgsinos (and other BSM particles) and a SM-like Higgs, but they are not unique in this regard. This scan populates an area of the $(m_{\tilde{\chi}_2^0}, \Delta m(\tilde{\chi}_2^0, \tilde{\chi}_1^0))$ plane roughly corresponding to

$$m_{\tilde{\chi}_2^0} \in [190, 300], \quad \Delta m(\tilde{\chi}_2^0, \tilde{\chi}_1^0) \in (0, 27] \text{ GeV}, \quad (9)$$

which turns out to be ideal for both the soft-lepton analyses and the dark matter (DM) relic abundance. The calculation of the MSSM mass spectrum, including electroweakino mixing matrices and decays, is handled using SARAH

	ATLAS wino/bino(+)	Decoupled higgsinos
$\{m_{\tilde{\chi}_1^0}, m_{\tilde{\chi}_2^0}, m_{\tilde{\chi}_1^\pm}\}$ [GeV]	{235, 250, 250}	{238.9, 255.6, 255.8}
$(N_{11}^2, N_{12}^2, N_{13}^2 + N_{14}^2)$	(0.9730, 0.0028, 0.0243)	(0.9991, 0.0004, 0.0005)
$(N_{21}^2, N_{22}^2, N_{23}^2 + N_{24}^2)$	(0.0099, 0.8928, 0.0972)	(0.0004, 0.9980, 0.0016)
$\tilde{\chi}_2^0$ decay modes (branching fraction)	$\tilde{\chi}_1^0 Z^* (100\%)$	$\tilde{\chi}_1^0 q\bar{q} (72.8\%)$
		$\tilde{\chi}_1^0 \nu\bar{\nu} (15.9\%)$
		$\tilde{\chi}_1^0 e^+e^- (3.98\%)$
		$\tilde{\chi}_1^0 \mu^+\mu^- (3.98\%)$
		$\tilde{\chi}_1^0 \tau^+\tau^- (3.27\%)$
$\tilde{\chi}_1^\pm$ decay modes (branching fraction)	$\tilde{\chi}_1^0 W^{-,*} (100\%)$	$\tilde{\chi}_1^0 \bar{u}d (66.8\%)$
		$\tilde{\chi}_1^0 e^-\bar{\nu}_e (11.3\%)$
		$\tilde{\chi}_1^0 \mu^-\bar{\nu}_\mu (11.3\%)$
		$\tilde{\chi}_1^0 \tau^-\bar{\nu}_\tau (10.6\%)$

Table 10 Comparison of neutralino mixings and decay modes in the ATLAS simplified bino-wino scenario [wino/bino(+)] and our decoupled-higgsinos scenario with bino-like LSP and wino-like NLSP.

[67–70], whose Fortran output code uses routines from the SPHENO [71, 72] library. We use a low-scale input card. Fermion masses are computed including loop corrections, while decays are handled at leading order. Higgs masses are computed including two-loop corrections [73–75]. BSMART keeps benchmark points in which the lightest CP-even scalar has mass $m_h \in [122, 128]$ GeV and the lightest neutralino is at least 50% bino, which is enforced by imposing the requirement $N_{11}^2 \geq 0.5$ on the bino- $\tilde{\chi}_1^0$ element of the neutralino mixing matrix. This requirement usually, but not always, picks out $M_1 < M_2$: the smallest $\Delta m(\tilde{\chi}_2^0, \tilde{\chi}_1^0)$ can be achieved for a bino-like LSP with M_1 a bit heavier than M_2 . Benchmark points with valid spectra are forwarded by BSMART to MICROMEGAS [76–78] for the calculation of the DM relic abundance and an estimate of direct-detection limits, which is performed at leading order using the CALCHEP [79] model files produced by SARAH for the MSSM. We discard points that are ruled out by direct searches, but in order to cover a suitable range of $\Delta m(\tilde{\chi}_2^0, \tilde{\chi}_1^0)$ we retain a number of points with both over- and underabundant dark matter. For each of these points, two SLHA cards are produced: one, with a real neutralino mixing matrix, is used as input for MG5_AMC along with a UFO model produced by SARAH; the other, with positive electroweakino mass eigenvalues, is used as input for RESUMMINO, which we use to compute the needed cross sections at next-to-next-to-leading order accuracy, including the resummation of QCD radiation at the next-to-next-to-leading (threshold) logarithmic accuracy (NNLO + NNLL). Finally, for all points surviving all prior constraints and the soft-lepton and monojet searches, we use HIGGSTOOLS [80] and SModelS [81–83] to perform a fast check for other experimental constraints. Points are kept only if the p -value inferred by BSMART from the HIGGSTOOLS

χ^2 calculation exceeds $p = 0.05$ (*i.e.*, there is no statistically significant difference between the signal model predictions and the experimental inputs used by HIGGSTOOLS) and the SModelS r -value is below $r = 1$.

The subtle differences between our bino-wino scenario and the ATLAS simplified wino/bino(+) scheme are shown in Table 10. There we record the physical light electroweakino masses and the light neutralinos’ gaugino and higgsino content, defined in terms of the elements of the neutralino mixing matrix; as well as the $\tilde{\chi}_2^0$ and $\tilde{\chi}_1^\pm$ branching fractions passed to MG5_AMC/PYTHIA 8. The left column reproduces this information from one of the wino/bino(+) SLHA cards used by the ATLAS Collaboration as input for MG5_AMC and made available on the HEPDATA repository for ATLAS-SUSY-2019-09.⁷ The right column reflects one of the points generated by our random scan with a mass spectrum similar to that of the ATLAS point. Inspection of all of the wino/bino(+) ATLAS cards reveals that ATLAS kept the mixing matrices and decay tables fixed and changed the masses by hand, which is artificial though acceptable for a simplified interpretation. As noted above, we instead compute the mixing matrices anew for each point. Also of note is the $O(1\text{--}10)\%$ higgsino content of the ATLAS neutralinos, as opposed to our stricter decoupled-higgsino scenario. Finally, we use the branching ratios for the three-body electroweakino decays computed by the SARAH-SPHENO workflow at leading order; ATLAS uses values either tabulated online⁸ or computed via other tools, but these are not specified in the provided cards. By comparing to the online tabulated values

⁷The available points can be found under “Resources” at <https://www.hepdata.net/record/ins1866951>.

⁸Found, for example, at <https://twiki.cern.ch/twiki/bin/view/LHCPhysics/SUSYCrossSections13TeVinosplit>.

we find that our branching ratios differ only by negligible amounts. As an aside, we note that the example parameter cards specify for each electroweakino a two-body decay to the appropriate (off-shell) weak boson with unit branching fraction, with in addition at least one *allowed* three-body decay (e.g., $\tilde{\chi}_2^0 \rightarrow \tilde{\chi}_1^0 e^+ e^-$) with *vanishing* branching fraction. This is the format used to force PYTHIA 8 to compute the branching fractions for the electroweakinos (although it cannot compute the matrix elements and therefore simulates the decays with a flat phase space). While such cards would be acceptable for the monojet searches (and, indeed, we use the PYTHIA 8 trick for those samples), the decay tables are ignored if using MADSPIN or our workflow in any case.

For our analysis toolchain we generate separate samples for the processes

$$pp \rightarrow \tilde{\chi}_2^0 \tilde{\chi}_1^\pm, \tilde{\chi}_2^0 \rightarrow \ell^+ \ell^- \tilde{\chi}_1^0$$

and $pp \rightarrow \tilde{\chi}_1^+ \tilde{\chi}_1^-$, (10)

as well as a “monojet sample” with $pp \rightarrow \tilde{\chi}_2^0 \tilde{\chi}_1^\pm, \tilde{\chi}_1^\pm \tilde{\chi}_1^\mp$ with no forced decay of the neutralino. In each case we allow matrix elements to include up to two additional partons and combine them according to the MLM merging prescription. We generate 3.2×10^6 events per sample per parameter point, of which we keep 110 for all analyses for this model. In similar fashion to the validation of the soft-lepton recasts, the generation is handled by BSMART creating gridpacks from MG5_AMC, which run on eight cores in parallel, passing their Les Houches Event samples to HACKANALYSIS for internal showering using PYTHIA 8, and finally for analysis. We use the package SPEY [84] to perform statistical analysis on our samples, including the calculation of expected and observed limits at 95% confidence level [85] and of discovery p -values.

3.2 Analysis & comparison to simplified bino-wino scenario

The results of our analysis of the bino-wino MSSM are displayed in Figure 8 and the accompanying Table 11. Figure 8 shows the expected and observed limits for all searches sensitive to this region of parameter space, as well as a light blue region in which the dark matter relic abundance lies within 20% of the observed value. It is first illustrative to compare our soft-lepton exclusions to those found for the simplified bino-wino model in the right panels of Figures 5 and 6. As expected they are very similar, with the only notable difference being the increased reach of the 2ℓ search at small Δm , since we do not include any statistical uncertainty on the signal in the statistics. Meanwhile, we are able to show expected and observed limits from the CMS monojet analysis, CMS-EXO-20-004, but not from its ATLAS equivalent: the

latter is much less sensitive and imposes no constraint on the parameter space visible here.

As advertised, both the 2ℓ and monojet channels are in mild but significant excess. Four statistically significant benchmark points are marked in Figure 8 and then detailed in Table 11. These points are chosen based on their statistics for either the ATLAS 2ℓ analysis *or* the CMS monojet (*i.e.*, there is no global fit), but we show the discovery significance and associated signal strength with respect to all four analyses for each point. In particular, there is a point with significant discovery p -value ($p < 0.05$) and another point with best-fit signal strength $\hat{\mu}$ close to unity for each of the 2ℓ and (CMS) monojet analyses. Here and throughout the rest of this work, the non-excluded point with $\hat{\mu}$ closest to unity is called “best-fit point” for that analysis; the point with the smallest discovery p -value is called “most significant”. For the MSSM, the point at $(m_{\tilde{\chi}_2^0}, \Delta m) = (273, 16.3)$ GeV, marked as “ATLAS 2ℓ best-fit point,” has a discovery p -value of $p = 0.047$ and an associated signal strength of $\hat{\mu} = 1.12$. It also shows some noteworthy significance, $p < 0.1$, with respect to the CMS monojet analysis, suggesting some overlap between excess regions. The “ATLAS 2ℓ most significant point” at $(m_{\tilde{\chi}_2^0}, \Delta m) = (284, 20.0)$ GeV, meanwhile, has $p = 0.041$ and $\hat{\mu} = 1.26$. The analogous points for the CMS monojet analysis are at $(m_{\tilde{\chi}_2^0}, \Delta m) = (287, 7.30)$ GeV, with $(p, \hat{\mu}) = (0.049, 1.15)$, and $(258, 11.8)$ GeV, with $(p, \hat{\mu}) = (0.044, 1.40)$. The best-fit point, with smaller Δm , is essentially invisible to the soft-lepton analyses, but the other point shows some improvement with larger Δm . We finally comment that the 2ℓ significant points, particularly the most significant point, lie within striking distance of the band preferred for the dark matter relic abundance, suggesting that this model interpretation, while imperfect, may provide a blueprint for constructing a new model dedicated to fitting these excesses.

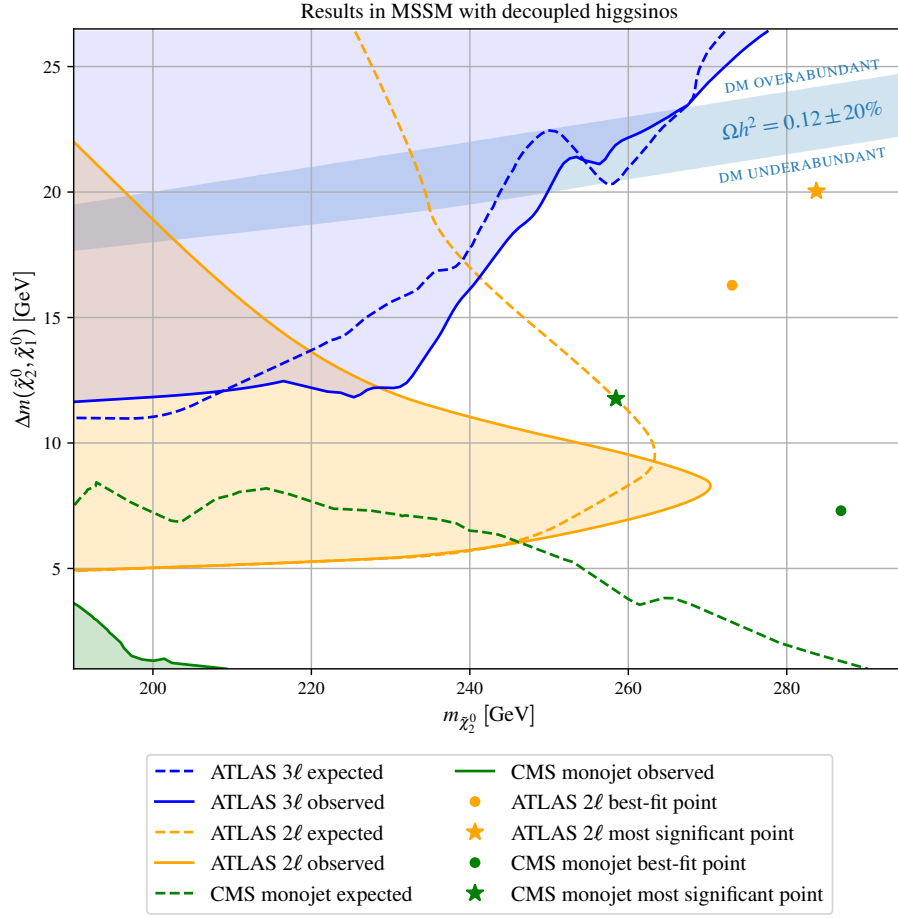


Fig. 8 View of the bino-wino MSSM parameter space relevant to the LHC excesses. Orange contours show limits from ATLAS-SUSY-2018-16 (2ℓ), while blue contours refer to ATLAS-SUS-2019-09 (3ℓ). Dashed contours show expected limits and solid contours denote the edge of the observed excluded regions, shaded correspondingly. The light blue band approximately indicates the parameter space region with relic abundance Ωh^2 within 20% of the *Planck* measurement. Two interesting non-excluded points are highlighted for each of the 2ℓ and monojet analyses.

Point ($m_{\tilde{\chi}_2^0}, \Delta m$) [GeV]	● ATLAS 2ℓ best fit (273, 16.3)	★ ATLAS 2ℓ most significant (284, 20.0)	● CMS monojet best fit (287, 7.30)	★ CMS monojet most significant (258, 11.8)
($p, \hat{\mu}$) [ATLAS 2ℓ]	(0.047, 1.12)	(0.041, 1.26)	(> 0.5, < 0.1)	(0.290, 0.30)
($p, \hat{\mu}$) [ATLAS 3ℓ]	(> 0.5, < 0.1)	(0.426, < 0.1)	(> 0.5, < 0.1)	(> 0.5, < 0.1)
($p, \hat{\mu}$) [CMS monojet]	(0.098, 1.58)	(0.065, 2.33)	(0.049, 1.15)	(0.044, 1.40)
($p, \hat{\mu}$) [ATLAS monojet]	(0.277, 1.21)	(0.163, 2.44)	(0.127, 1.53)	(0.277, 0.879)
M_1 [GeV]	248.0	254.6	269.9	238.2
M_2 [GeV]	241.7	251.3	254.0	228.6
m_h [GeV]	127.0	126.5	126.8	126.8
$m_{\tilde{\chi}_1^0}$ [GeV]	256.8	263.7	279.5	246.7
$m_{\tilde{\chi}_2^0}$ [GeV]	273.1	283.7	286.8	258.4
$m_{\tilde{\chi}_1^\pm}$ [GeV]	273.3	283.9	287.0	258.6
($N_{11}, N_{12}, N_{13}, N_{14}$)	(0.9995, -0.0211, 0.0232, -0.0038)	(0.9996, -0.0175, 0.0231, -0.0039)	(0.9984, -0.0501, 0.02443, -0.0043)	(0.9993, -0.0284, 0.0235, -0.0038)
($N_{21}, N_{22}, N_{23}, N_{24}$)	(0.0220, 0.9990, -0.0392, 0.0066)	(0.0184, 0.9990, -0.0394, 0.0068)	(0.0511, 0.9979, -0.0386, 0.0068)	(0.0293, 0.9988, -0.0390, 0.0063)

Table 11 Statistics and benchmark information for significant MSSM points marked in Figure 8. The significance and associated signal strength ($p, \hat{\mu}$) are provided for all four analyses for each point. Note that ATLAS monojet sensitivity can only be computed based on the most sensitive individual signal region. All BSM particles not listed here are decoupled to at least 2 TeV.

4 Alternative interpretation: NMSSM with singlino-higgsino LSP

The Next-to-Minimal Supersymmetric Standard Model [86] (NMSSM) extends the MSSM field content to include a superfield S that transforms as a singlet under the SM gauge group. A signature feature of this model is the appearance of a superpotential coupling between S and the Higgs superfields that can take the place of the MSSM μ term after enforcing a \mathbb{Z}_3 symmetry forbidding all gauge-invariant dimensionful superpotential contributions. To be specific, the MSSM superpotential is modified according to

$$\mathcal{W}_{\text{MSSM}} \supset \mu \mathcal{H}_u \mathcal{H}_d \rightarrow \mathcal{W}_{\text{NMSSM}} \supset \lambda S \mathcal{H}_u \mathcal{H}_d + \frac{1}{3} \kappa S^3, \quad (11)$$

and the corresponding soft scalar terms go as

$$V_{\text{MSSM}}^{\text{soft}} \supset b \mu \mathcal{H}_u \mathcal{H}_d \rightarrow V_{\text{NMSSM}}^{\text{soft}} \supset A_\lambda \lambda S \mathcal{H}_u \mathcal{H}_d + \frac{1}{3} A_\kappa \kappa S^3. \quad (12)$$

The $S \mathcal{H}_u \mathcal{H}_d$ term in (11) generates an effective μ term when the singlet scalar S obtains a vacuum expectation value (VEV). The NMSSM can thus solve the so-called “ μ problem” of the MSSM if $\mu_{\text{eff}} = \lambda \langle S \rangle$ is at the weak scale [87]. In the CP-conserving limit, the addition of the singlet scalar leads to a physical scalar sector composed of two CP-odd and three CP-even neutral scalars in addition to the familiar charged scalars of the MSSM. Generically, the SM-like Higgs need not be the lightest CP-even scalar and the phenomenology of the NMSSM’s scalar sector alone can hence be quite rich. The electroweakino sector is likewise augmented to include an additional neutralino, which can be light.

There is a particularly interesting NMSSM scenario in which the LSP is composed mostly of the singlet fermion (singlino) and μ_{eff} is at the weak scale such that the next-lightest electroweakinos are predominantly higgsinos (see also [6, 7, 12] for a discussion of the soft-lepton searches in this context). In this *singlino-higgsino* scenario there are four light electroweakinos $\{\tilde{\chi}_1^0, \tilde{\chi}_2^0, \tilde{\chi}_1^\pm, \tilde{\chi}_3^0\}$, nearly aligned with the singlino and triplet of higgsinos. This spectrum opens new channels relevant to the LHC excesses that we are studying, including for instance the process $pp \rightarrow \tilde{\chi}_2^0 \tilde{\chi}_3^0$ with both higgsinos decaying to $\tilde{\chi}_1^0$ via Z bosons (which may be off shell if the singlino-higgsino spectrum is sufficiently compressed). On the other hand, production of the LSP itself has quite low cross sections insofar as $\tilde{\chi}_1^0$ is dominated by the singlino. Meanwhile, notably, this scenario also has parameter space predicting the correct dark matter relic abundance through freeze out. The dominant annihilation channels are of singlinos to weak bosons, $\tilde{\chi}_1^0 \tilde{\chi}_1^0 \rightarrow W^+ W^- / ZZ$, and singlino-higgsino coannihilations to quarks,

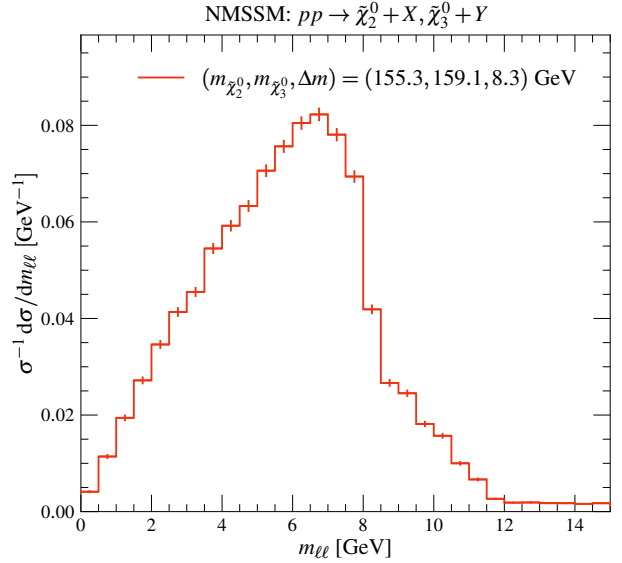


FIG. 9 $m_{\ell\ell}$ distribution for the NMSSM with a singlino-like LSP as found from our simulations for the processes $pp \rightarrow \tilde{\chi}_2^0 + X$ and $pp \rightarrow \tilde{\chi}_3^0 + Y$, where $X \in \{\tilde{\chi}_1^\pm, \tilde{\chi}_3^0\}$ and $Y \in \{\tilde{\chi}_1^\pm, \tilde{\chi}_2^0\}$, with matrix elements including up to two additional partons. Here $\Delta m = m_{\tilde{\chi}_2^0} - m_{\tilde{\chi}_1^0}$, as for the MSSM.

e.g. $\tilde{\chi}_1^0 \tilde{\chi}_1^- \rightarrow \bar{u}d$. The contributions of higgsino coannihilations like $\tilde{\chi}_{2,3}^0 \tilde{\chi}_1^- \rightarrow \bar{u}d$ are subleading but non-negligible.

4.1 Parameter space scan and event generation

As for our study of the MSSM, we use BSMART to perform a random scan of the parameter space possibly relevant to the soft-lepton and monojet searches. In the interest of exploring both the collider excesses and the DM relic abundance, we require that the LSP be at least 90% singlino, which implies the condition $|N_{15}|^2 \geq 0.90$ on the $\tilde{\chi}_1^0$ -singlino element of the neutralino mixing matrix. We look for $\{\tilde{\chi}_2^0, \tilde{\chi}_1^\pm, \tilde{\chi}_3^0\}$ with similarly high higgsino content. Since these electroweakinos are higgsino-like, we target a similar region of the $(m_{\tilde{\chi}_2^0}, \Delta m \equiv \Delta m(\tilde{\chi}_2^0, \tilde{\chi}_1^0))$ plane as seen in Section 2 for the ATLAS soft-lepton analyses; namely,

$$m_{\tilde{\chi}_2^0} \in [150, 220] \text{ GeV}, \quad \Delta m(\tilde{\chi}_2^0, \tilde{\chi}_1^0) \in (0, 25] \text{ GeV}, \quad (13)$$

though not quite all of this Δm slice is probed in practice. As before, the mass spectrum, mixing matrices, and decays are calculated by SPHENO, with fermion (Higgs) masses at one-loop (two-loop) accuracy and decays at tree level. The dark matter relic abundance is computed by MICROMEGAS, including LSP coannihilations and NLSP (co)annihilations, and the usual range of experimental constraints are imposed by HIGGSTOOLS and SModelS for points appearing to inhabit the soft-lepton/monojet excess region. The lightest CP-even scalar is required to have mass $m_h \in [122, 128] \text{ GeV}$.

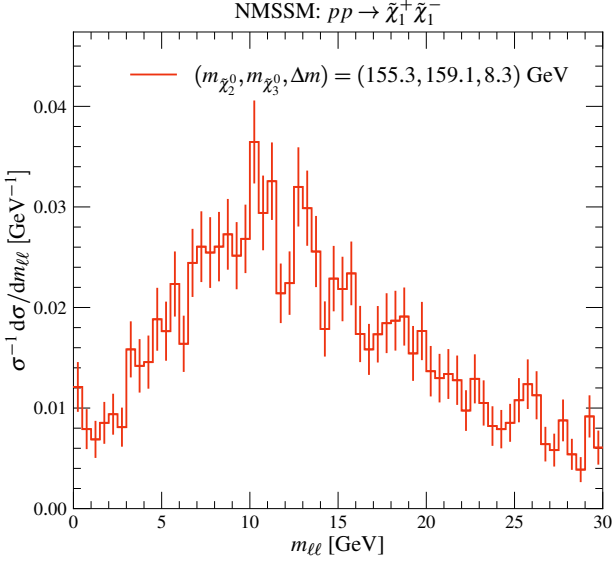


FIG. 10 $m_{\ell\ell}$ distribution for the NMSSM with a singlino-like LSP as found from our simulations for the chargino pair-production process $pp \rightarrow \tilde{\chi}_1^+ \tilde{\chi}_1^-$, with matrix elements including up to two additional partons.

For this scan we again run Fortran code created with SARAH linked to the SPHENO library, with a low-scale input card. We solve the tadpole equation for the singlet scalar in order to use μ_{eff} instead of the singlet VEV $\langle S \rangle$ as an input. The full set of variable inputs includes the Higgs sector parameters

$$\begin{aligned} \mu_{\text{eff}} &\in [100, 250] \text{ GeV}, \\ \kappa &\in [1, 20] \times 10^{-3}, \\ \delta &\in [0.01, 0.20] \text{ such that } \lambda = (2 + \delta)\kappa, \\ \tan \beta &\in [8, 20] \end{aligned} \quad (14)$$

and the soft (s)fermion SUSY-breaking parameters

$$\begin{aligned} M_t^2 &\in [2.5, 10] \times 10^7 \text{ GeV}^2, \\ A_t &\in [-5, 5] \times 10^3 \text{ GeV}, \\ A_\lambda &\in [-3, 3] \times 10^2 \text{ GeV}, \\ A_\kappa &\in [-3, 3] \times 10^2 \text{ GeV}; \end{aligned} \quad (15)$$

while the other relevant parameters are fixed as follows:

$$\begin{aligned} M_1 = M_2 &= 2 \text{ TeV}, \\ M_{\tilde{q}\tilde{q}^\dagger}^2 &= (8.25 \times 10^8, 8.25 \times 10^8) \text{ GeV}^2, \\ M_{\tilde{u}}^2 = M_{\tilde{d}}^2 &= (8.25 \times 10^8, 8.25 \times 10^8, 1.25 \times 10^7) \text{ GeV}^2, \\ M_{\tilde{e}}^2 = M_{\tilde{\nu}_\tau}^2 &= (4.25 \times 10^8, 4.25 \times 10^8, 4.25 \times 10^6) \text{ GeV}^2. \end{aligned} \quad (16)$$

The requirement that $\lambda \gtrsim 2\kappa$ arises from the need for a singlino-like LSP and $O(10)$ GeV compression between the singlino-dominated state and the higgsinos. The relic abundance turns out to be sensitive to the deviation δ from

the exact relation $\lambda = 2\kappa$, with $\delta \approx 0.07$ producing the majority of points with $\Omega h^2 \approx 0.12$. Our collection includes points with larger δ , which have overabundant DM with relic densities as high as $\Omega h^2 = 0.2$, in order to better cover the range of Δm values relevant to the LHC discussion.

For our analysis toolchain, in a similar way as for the MSSM points, we generate three separate samples involving off-shell Z decays to leptons; purely off-shell W decays to leptons; and a separate monojet sample with flat ($|\mathcal{M}|^2 \rightarrow 1$) decays handled by PYTHIA 8. As mentioned above, the higgsino-like $\tilde{\chi}_2^0$ and $\tilde{\chi}_3^0$ are both light and can decay via off-shell Z bosons, which leads to a complicated set of processes. This is interesting in itself: in the basis where the neutralino mixing matrix is real, it turns out that our $\tilde{\chi}_2^0$ has positive mass (as does $\tilde{\chi}_1^0$) while $\tilde{\chi}_3^0$ has the opposite. In keeping with the discussion in Section 2.1, this spectrum suggests that $\tilde{\chi}_2^0$ decays with an $m_{\ell\ell}$ distribution similar to the ATLAS wino/bino(+) scenario, while $\tilde{\chi}_3^0$ decays like a higgsino. This expectation is borne out in Figure 9 for a typical point produced by our scan: by comparison with Figure 2, one can make out in Figure 10 the linear combination of $\tilde{\chi}_2^0$ and $\tilde{\chi}_3^0$ $m_{\ell\ell}$ distributions. Due to the complexity of the multicomponent signal, we use the leading-order cross sections reported by MG5_AMC and PYTHIA 8 after MLM merging (with merging scale set again to 40 GeV). We perform simulations for 194 parameter points for the soft-lepton analyses. The generation of the monojet sample(s) involves the production of all possible pairs of light electroweakinos, and relies on matrix elements featuring up to two additional partons. It is worth noting that the $pp \rightarrow \tilde{\chi}_1^+ \tilde{\chi}_1^-$ samples are relatively simple and the subsequent $m_{\ell\ell}$ distribution, shown for our example point in Figure 10, is similar to the chargino-pair distributions for the MSSM shown in Figure 4. For the monojet analyses we simulate 238 parameter points. As before, we generate 3.2×10^6 events per sample per parameter point. The generation is handled by BSMART creating grid-packs from MG5_AMC, which run on eight cores in parallel, passing their Les Houches Event samples to HACKANALYSIS for showering, analysis, and statistics. Our simulation relies on a UFO model produced by SARAH.

4.2 Analysis: Degraded monojet fit

The results of our NMSSM analysis are displayed in Figure 11 and the accompanying Table 12. Figure 11 shows the expected and observed limits from the soft-lepton analyses, which are the only searches sensitive to this part of the $(m_{\tilde{\chi}_2^0}, \Delta m)$ plane. In particular, both monojet analyses are markedly less sensitive to this model than to the decoupled-higgsino MSSM; neither search excludes any of the points in our scan. This reduced sensitivity degrades the overlap between the monojet excesses (which do still appear in the form of weaker observed limits on the monojet signal strength) and

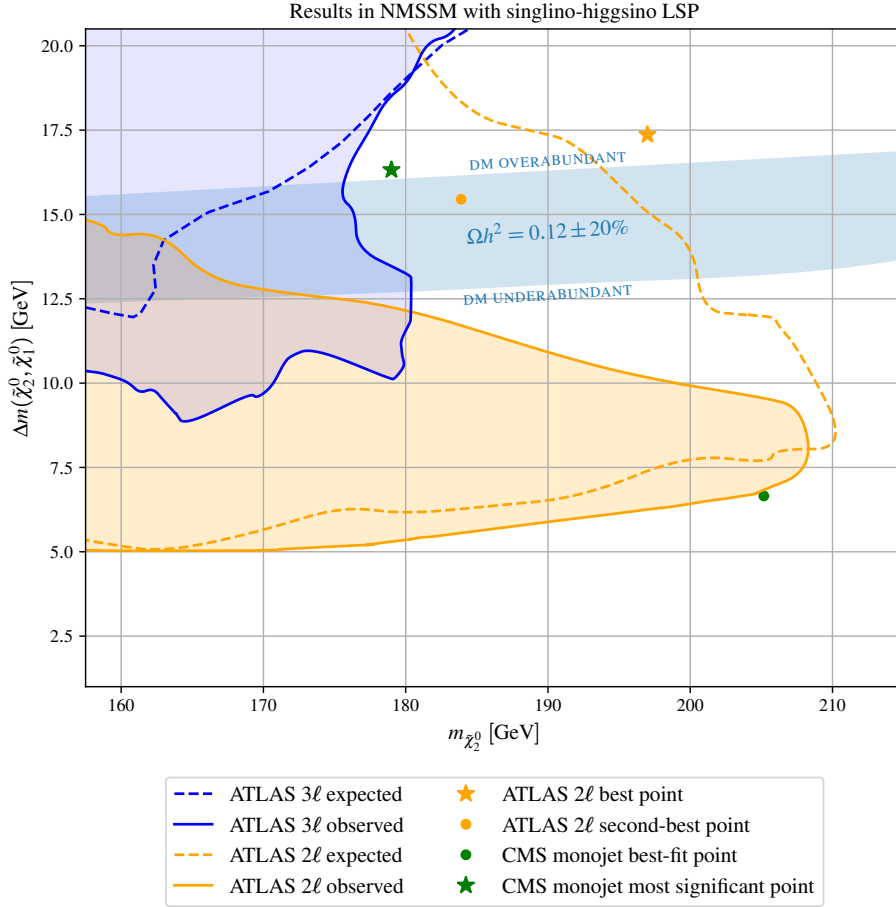


Fig. 11 View of NMSSM parameter space relevant to the LHC excesses. Orange contours show limits from ATLAS-SUSY-2018-16 (2ℓ), while blue contours refer to ATLAS-SUS-2019-09 (3ℓ). Dashed contours show expected limits and solid contours denote the edge of the observed excluded regions, shaded correspondingly. The light blue band indicates approximately the region of the parameter space with relic abundance Ωh^2 within 20% of the *Planck* measurement. Two interesting non-excluded points are highlighted for each of the 2ℓ and monojet analyses.

the 2ℓ excess, and causes strong tension between the monojet discovery p -values and best-fit signal strengths. Figure 11 also shows that, unlike in the MSSM, the observed limit from ATLAS-SUSY-2019-09 is mostly stronger than the expected limit.

Despite the lack of a limit from either monojet search, we report four statistically significant benchmark points in Table 12. As for the MSSM, we report the discovery significance and associated signal strength for all four analyses for each point. The non-excluded point with the greatest significance with respect to the 2ℓ analysis is at $(m_{\tilde{\chi}_2^0}, \Delta m) = (197, 17.4)$ GeV; it carries a discovery p -value of $p = 0.041$ associated with a signal strength of $\hat{\mu} = 0.97$. Here already we can see the tension with the CMS monojet analysis, which requires more than thrice our yield for meaningful discovery potential. Another interesting point with high significance lies at $(m_{\tilde{\chi}_2^0}, \Delta m) = (183.9, 15.5)$ GeV, with $p = 0.044$ and $\hat{\mu} = 0.80$. The fit at this point is imperfect, but it lies within the band predicting a reasonable DM relic abundance. Meanwhile, for the CMS monojet analysis, the non-excluded

point⁹ with the best fit¹⁰ is at $(m_{\tilde{\chi}_2^0}, \Delta m) = (205, 6.66)$ GeV and has $\hat{\mu} = 1.914$ with $p = 0.712$. This point is a poor fit for both soft-lepton excesses. The (non-excluded) monojet point with greatest significance, on the other hand, is at $(m_{\tilde{\chi}_2^0}, \Delta m) = (179, 16.3)$ GeV; its discovery p -value is $p = 0.051$, but the associated signal strength is $\hat{\mu} = 3.791$, suggesting a severe deficit of monojet events at this point. Altogether, we find a strong contrast between the global picture in the bino-wino MSSM (which shows some overlap between statistically significant monojet and 2ℓ excesses) and the NMSSM, which exhibits a better fit between the 2ℓ excess and the DM relic abundance at the expense of the monojet fit.

⁹We are now discussing the sensitivity of the monojet analysis, but the limiting search is invariably one of the soft-lepton analyses, so by “non-excluded” we mean allowed by one of those.

¹⁰For the NMSSM monojet results, we require $\hat{\mu} < 4$ in order to limit ourselves to points with somewhat reasonable fits.

Point ($m_{\tilde{\chi}_2^0}, \Delta m$) [GeV]	★ ATLAS 2ℓ best (197, 17.4)	● ATLAS 2ℓ second best (184, 15.5)	● CMS monojet best fit (205, 6.66)	★ CMS monojet most significant (179, 16.3)
($p, \hat{\mu}$) [ATLAS 2ℓ]	(0.041, 0.97)	(0.044, 0.80)	(0.435, < 0.1)	(0.071, 0.64)
($p, \hat{\mu}$) [ATLAS 3ℓ]	(0.446, 0.12)	(> 0.5, 0.12)	(> 0.5, 0.71)	(> 0.5, 0.13)
($p, \hat{\mu}$) [CMS monojet]	(0.132, 3.00)	(0.129, 2.65)	(0.712, 1.91)	(0.051, 3.79)
($p, \hat{\mu}$) [ATLAS monojet]	(0.277, 2.44)	(0.277, 2.02)	(0.127, 2.96)	(0.277, 2.08)
μ_{eff} [GeV]	189.3	177.0	199.1	172.6
κ	0.0157	0.0108	0.0025	0.0146
λ	0.0330	0.0226	0.0050	0.0309
$\tan\beta$	19.71	25.94	10.70	12.82
M_t^2 [GeV ²]	8.06×10^7	7.20×10^7	3.42×10^7	9.12×10^7
A_t [GeV]	2.61×10^3	-1.28×10^3	2.07×10^3	-2.64×10^3
A_λ [GeV]	-34.60	-92.77	189.4	192.0
A_κ [GeV]	-43.01	-8.771	-161.3	-55.91
m_h [GeV]	124.0	123.4	123.0	122.6
$m_{\tilde{\chi}_1^0}$ [GeV]	179.6	168.5	198.5	162.7
$m_{\tilde{\chi}_2^0}$ [GeV]	197.0	183.9	205.2	179.0
$m_{\tilde{\chi}_1^\pm}$ [GeV]	198.1	185.5	207.1	180.3
$m_{\tilde{\chi}_3^0}$ [GeV]	199.9	187.3	209.0	182.1
($N_{11}, N_{12}, N_{13}, N_{14}, N_{15}$)	(0.0042, -0.0070, 0.1547, -0.1683, 0.9735)	(0.0032, -0.0053, 0.1201, -0.1299, 0.9841)	(0.0016, -0.0026, 0.0580, -0.0597, 0.9965)	(0.0041, -0.0069, 0.1479, -0.1622, 0.9756)
($N_{21}, N_{22}, N_{23}, N_{24}, N_{25}$)	(-0.0173, 0.0289, -0.6932, 0.6827, 0.2284)	(-0.0172, 0.0287, -0.7004, 0.6907, 0.1767)	(-0.0184, 0.0312, -0.7077, 0.7006, 0.0832)	(-0.0176, 0.0294, -0.6951, 0.6838, 0.0219)
$\text{Im}(N_{31}, N_{32}, N_{33}, N_{34}, N_{35})$	(-0.0134, 0.0226, 0.7039, 0.7097, 0.0110)	(-0.0137, 0.0231, 0.7036, 0.7101, 0.0080)	(-0.0126, 0.0216, 0.7041, 0.7097, 0.0016)	(-0.0131, 0.0220, 0.7035, 0.7100, 0.0116)

Table 12 Statistics and benchmark information for significant NMSSM points marked in Figure 11. The significance and associated signal strength ($p, \hat{\mu}$) are provided for all four analyses for each point. Neutralino masses are forced positive such that the $\tilde{\chi}_3^0$ mixing matrix elements N_{3i} (with $i = 1, 2, \dots, 5$) are imaginary.

5 Non-supersymmetric interpretations

Having shown that two supersymmetric scenarios give fits of varying quality to the soft-lepton and monojet excesses, we now consider whether some non-supersymmetric model might be compatible with either or both. Two well motivated frameworks capable of producing events with the correct final states include scalar dark matter coupling to the Standard Model with a vector-like lepton [88] and a Higgs triplet model originally proposed to generate neutrino masses [89–94]. Here we briefly review each scenario and describe our scans over their relevant parameter spaces.

5.1 Scalar dark matter with vector-like leptons

One class of simplified dark matter models features scalar or fermionic DM coupling directly to a SM lepton and a mediating field with identical SM gauge quantum numbers [88]. We focus on scenarios with scalar dark matter χ interacting with vector-like mediating lepton(s) (VLLs). In principle, the dark matter could couple to right- or left-handed SM leptons along with some suitable new VLL field(s). In the first case, the VLL would have SM quantum numbers $(\mathbf{1}, \mathbf{1}, -1)$; in the second case it must lie in the representation $(\mathbf{1}, \mathbf{2}, -\frac{1}{2})$. In the singlet VLL case, events with an opposite-charge lepton pair,

missing energy, and jets can result from VLL pair production and decay, as depicted in Figure 12. The invariant mass of the $\ell^+ \ell^-$ pair can be low if the mass splitting $\Delta m(\ell', \ell)$ is small, of $\mathcal{O}(1-10)$ GeV. On the other hand, a monojet signature is unlikely to arise in this model unless the SM leptons are too soft to be observed. The doublet VLL model, on the other hand, can produce *both* soft-lepton events in the same topology as the singlet VLL model *and* monojet events via pair production of the electrically neutral ν' , as shown in Figure 13. Therefore we expect that the doublet VLL model may be the better choice for the excesses in question, and we focus on this scenario in our analysis. For a single flavor of doublet VLL, the most general DM-VLL interaction Lagrangian can be written as

$$\mathcal{L} \supset \lambda_I \chi \bar{\Psi} L_I + \text{H.c.}, \quad (17)$$

where Ψ denotes a weak doublet of vector-like leptons and L_I with $I \in \{1, 2, 3\}$ is a SM lepton weak doublet, with the parameter λ representing a vector of VLL couplings in the flavor space. Regarding global symmetries, we suppose that (despite the name) the VLL fields do not carry lepton number. Lepton number is instead conserved because the complex scalar χ carries $L = -1$. We therefore neglect mixing between the VLL and any SM lepton. Meanwhile, if the dark matter and VLL(s) are odd under a \mathbb{Z}_2 symmetry under which all SM fields have even parity, then χ is a viable dark

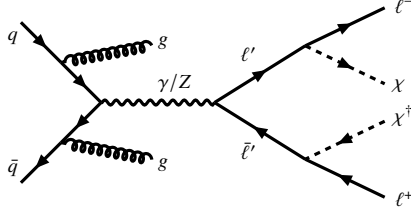


FIG. 12 Soft-lepton signal from pair production of a vector-like charged lepton ℓ' at the LHC, followed by the direct decay of each ℓ' to a SM lepton ℓ and the DM particle χ .

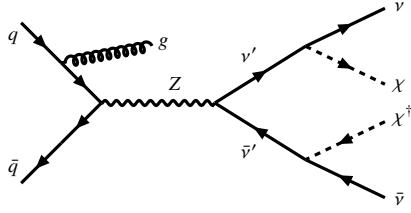


FIG. 13 Monojet signal from pair production of the vector-like neutrino ν' at the LHC, followed by the direct decay of each ν' to a SM neutrino ν and the DM particle χ .

matter candidate as long as χ is lighter than the VLL(s), as in all t -channel DM simplified models.

To fix notation, let the VLL doublet have components denoted by $\Psi = (\nu', \ell')^\top$ in analogy with the SM doublets $L_I = (\nu_{LI}, \ell_{LI})^\top$. The operator (17) then produces the couplings

$$\mathcal{L} \supset \lambda_I \chi (\bar{\nu}' \nu_{LI} + \bar{\ell}' \ell_{LI}) + \text{H.c.} \quad (18)$$

Meanwhile, the Ψ kinetic terms include $\bar{\nu}' \nu' / \bar{\ell}' \ell' (\gamma/Z)$ and $\bar{\nu}' \ell' W^+$ interactions. The latter coupling seems interesting because it provides a distinct decay channel for one component of Ψ that can produce a soft lepton through its decay via an off-shell W boson, but in practice this W -mediated three-body decay is always dominated by the Yukawa-like two-body decays from (18).

It is of course interesting to consider the phenomenology of the dark matter candidate χ . Its annihilation is dominated by t -channel diagrams to pairs of SM leptons and neutrinos, mediated by their heavy partners, but in the parameter space regions that we consider, coannihilations of χ with the vector-like particles and annihilations of the VLLs themselves are quite efficient. Many processes in the latter category are moreover proportional to gauge couplings and thus cannot be controlled by our choices of Yukawa-like couplings λ_I . Therefore, as we show below, not only does the *Planck* relic abundance favor quite small values of λ_I (of $\mathcal{O}(10^{-3})$, which seems to escape direct-detection constraints [88, 95]), but in fact the *Planck* value seemingly cannot be attained for arbitrarily small mass splittings between the VLLs and the dark matter.

We perform an enhanced scan with 9.6×10^6 events per point, simulating pair production of vector-like leptons

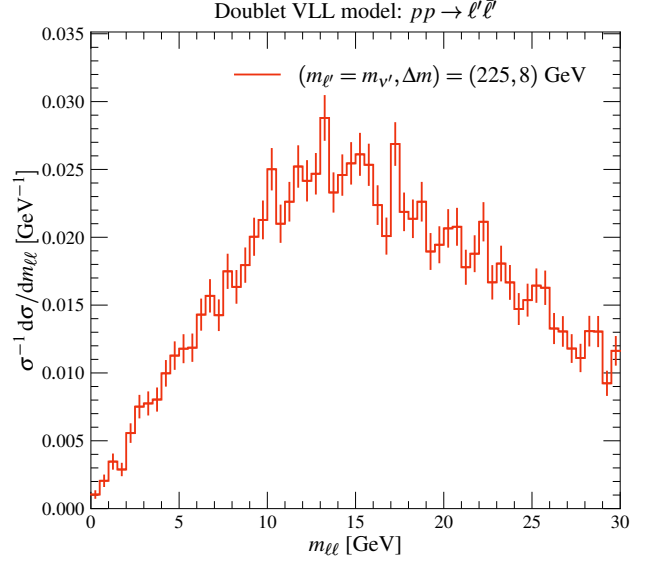


FIG. 14 $m_{\ell\ell}$ distribution resulting from the production and decay of a pair of doublet vector-like leptons, $pp \rightarrow \ell' \bar{\ell}' \rightarrow \ell^+ \ell^- \chi \chi$, after combining matrix elements featuring up to two additional partons. We consider a scenario with a vector-like lepton mass of 225 GeV and dark matter scalar mass of 217 GeV.

relying on matrix elements including up to two additional partons. Event generation is performed by MG5_AMC using a UFO module produced by FEYNRULES [96, 97] based on our own implementation of the doublet VLL model. In order to run the recast of the monojet search at the same time, we simulate $pp \rightarrow \bar{\ell}' \nu'$ and $pp \rightarrow \bar{\nu}' \nu'$ events in the same samples. We fix the branching ratios of ℓ' to be 50% to electrons plus dark matter, 50% to muons plus dark matter; and of ν' entirely to neutrinos plus dark matter. We first performed simulations for 131 parameter points in this model, which sufficed for the soft-lepton analyses, and added 44 more points in order to improve coverage of the $(m_{\ell'}, \Delta m)$ plane for the monojet analyses. In Figure 14 we show the $m_{\ell\ell}$ distribution of events in our data, which shows a peak at roughly $2\Delta m$ but is much broader and with a longer tail than for the three-body decay processes that we have considered so far. We finally note that the dark matter relic abundance is computed for these benchmark points at leading order by MADDM [98–100], which is convenient since it obviates the need to produce a separate input for MICROMEGAS. Since the VLL branching fractions are fixed to the desired values simply by setting $\lambda_1 = \lambda_2$ and their size is irrelevant for the collider study, these are fixed for event generation but allowed to vary as we search for parameter space predicting the correct DM relic abundance.

The results of our scan of the VLL doublet model are displayed in Figure 15 and the accompanying Table 13. Figure 15 is quite different from Figures 8 and 11, which reflects the unique physics of this non-supersymmetric model. We first see that the ATLAS 2ℓ search is not at all in excess for this

model; accordingly, there are no points with high discovery significance for that analysis. (The 3ℓ analysis is insensitive to this model by construction: there are no processes producing three leptons.) This behavior is at least partially due to the $m_{\ell\ell}$ distributions characteristic of this model: as noted above, the vector-like leptons tend to produce leptons hard enough to populate bins of the ATLAS-SUSY-2018-16 analysis in which underfluctuations are reported, and which by themselves can powerfully exclude models predicting even a few high- $m_{\ell\ell}$ events.

On the other hand, the monojet excess does survive for this model, so we report two statistically significant points associated with this analysis in Table 13. There is a point with good significance for the CMS monojet search at $(m_{\ell'}, \Delta m(\ell', \chi)) = (150, 2)$ GeV, which has $p = 0.0322$ and $\hat{\mu} = 1.097$. There is a nearby point with a slightly better fit at $(m_{\ell'}, \Delta m) = (130, 3)$ GeV; it has $p = 0.0454$ and $\hat{\mu} = 1.071$. For illustrative purposes, as for previous models, we include in Figure 15 a band in which the dark matter relic abundance (computed at leading order by MADDM) lies within 20% of the observed value by the Planck Collaboration for a benchmark with $\lambda_1 = \lambda_2 = 5 \times 10^{-3}$. As noted above, it is not possible to achieve the correct relic abundance in the vicinity of the monojet points. Coannihilations with ℓ' and ν' , most of which are of electroweak strength and independent of the Yukawa-like couplings λ_I , are too efficient when the mass splittings are of $\mathcal{O}(1)$ GeV, rendering χ underabundant. We note that the scalar DM annihilation cross section is significantly enhanced at next-to-leading order by three-body processes featuring the emission of a photon (*e.g.*, $\chi\chi \rightarrow \ell^+\ell^-\gamma$); the NLO corrections to our results, in this regime where $m_{\ell'}/m_\chi \approx (1.0, 1.25)$, can be of $\mathcal{O}(10)\%$ [101, 102].

5.2 Additional scalars in the type-II seesaw model

Another longstanding problem, the origin of neutrino masses, is addressed by the type-II seesaw model [89–94], which provides a UV completion of the Weinberg operator

$$\mathcal{L}_{\text{Weinberg}} = \epsilon_{ij}\epsilon_{kl}\bar{L}_i^c L_j \Phi_k \Phi_l, \quad (19)$$

where Φ and L represent the SM Higgs and lepton doublets [103]. The type-II seesaw model adds to the Standard Model a $Y = 1$ weak-triplet scalar Δ that can be parameterized as

$$\Delta = \frac{1}{\sqrt{2}} \begin{pmatrix} \Delta^+ & \sqrt{2}\Delta^{++} \\ \sqrt{2}\Delta^0 & -\Delta^+ \end{pmatrix}. \quad (20)$$

The scalar potential is given by

$$V(\Phi, \Delta) = -m_\Phi^2 \Phi^\dagger \Phi + \frac{1}{4} \lambda (\Phi^\dagger \Phi)^2 + m_\Delta^2 \text{tr} \Delta^\dagger \Delta \\ + (\mu \Phi^\dagger i \sigma^2 \Delta^\dagger \Phi + \text{H.c.}) + \lambda_1 \Phi^\dagger \Phi \text{tr} \Delta^\dagger \Delta \\ + \lambda_2 (\text{tr} \Delta^\dagger \Delta)^2 + \lambda_3 \text{tr} (\Delta^\dagger \Delta)^2 + \lambda_4 \Phi^\dagger \Delta \Delta^\dagger \Phi. \quad (21)$$

The physical scalars comprise two CP-even scalars h, S , two CP-odd scalars G^0, A (G^0 becoming the longitudinal mode of the Z boson), two singly charged scalars G^\pm, S^\pm (G^\pm becoming the longitudinal mode of W^\pm), and a doubly charged scalar $S^{\pm\pm}$. All physical states except the doubly charged scalar are mixtures of the components of the SM-like weak doublet Φ and of the triplet Δ . It has been pointed out [104] that relatively light charged scalars in this model are experimentally allowed when the mixing between Δ and Φ is small (so that the charged scalars decay predominantly via W bosons) and when the hierarchy of CP-even scalars is $\{S^{\pm\pm}, S^\pm, S\}$ in order of decreasing mass. At tree level, the mass splittings between scalars satisfy the relation

$$m_{S^{\pm\pm}}^2 - m_{S^\pm}^2 = m_{S^\pm}^2 - m_S^2 = -\frac{1}{4} \lambda_4 v^2, \quad (22)$$

so that $S^{\pm\pm}$ is the heaviest scalar only if $\lambda_4 < 0$. Meanwhile, if the triplet VEV v_Δ is small enough, one or both of the electrically neutral scalars $\{S, A\}$ decays almost entirely to neutrinos. Thus in scenarios exhibiting small scalar mixing and low v_Δ , the type-II seesaw model can generate events with soft leptons and missing energy through scalar pair production. An example process is shown in Figure 16. But it is immediately apparent that pair production of the doubly charged scalar may produce additional soft jets or leptons that may be rejected by the search criteria.

We perform a scan over $m_{S^{\pm\pm}} \in [100, 200]$ GeV and $\Delta m \in [1, 30]$ GeV. As usual, we use the MG5_AMC package; in this case the input UFO is produced using the publicly available FEYNRULES implementation of the type-II seesaw model [105]. We simulate all at once the processes

$$pp \rightarrow AS, AS^\pm, S^\pm S, S^\pm S^\mp, S^{\pm\pm} S^\mp, S^{\pm\pm} S^{\mp\mp}; \quad (23)$$

with matrix elements including up to two additional partons. This is a large number of processes, and we cannot use generator biases because of the mix of final states, so we generate 2×10^7 events for each of 215 parameter points for all analyses. We show the total $m_{\ell\ell}$ distribution found in an event sample with $m_{S^{\pm\pm}} = 170$ GeV, $m_{S^\pm} = 162$ GeV in Figure 17. Since we select only pairs of leptons with opposite signs, the topologies are similar to those of chargino pair production, but with BSM scalars instead of fermions. The $m_{\ell\ell}$ distribution is thus similar to that case, with a peak around $\Delta m = m_{S^\pm} - m_S$. In the end, we find total cross sections of $\mathcal{O}(1)$ pb, yet the efficiencies for any given signal region are barely more than 10^{-6} for the soft-lepton analysis:

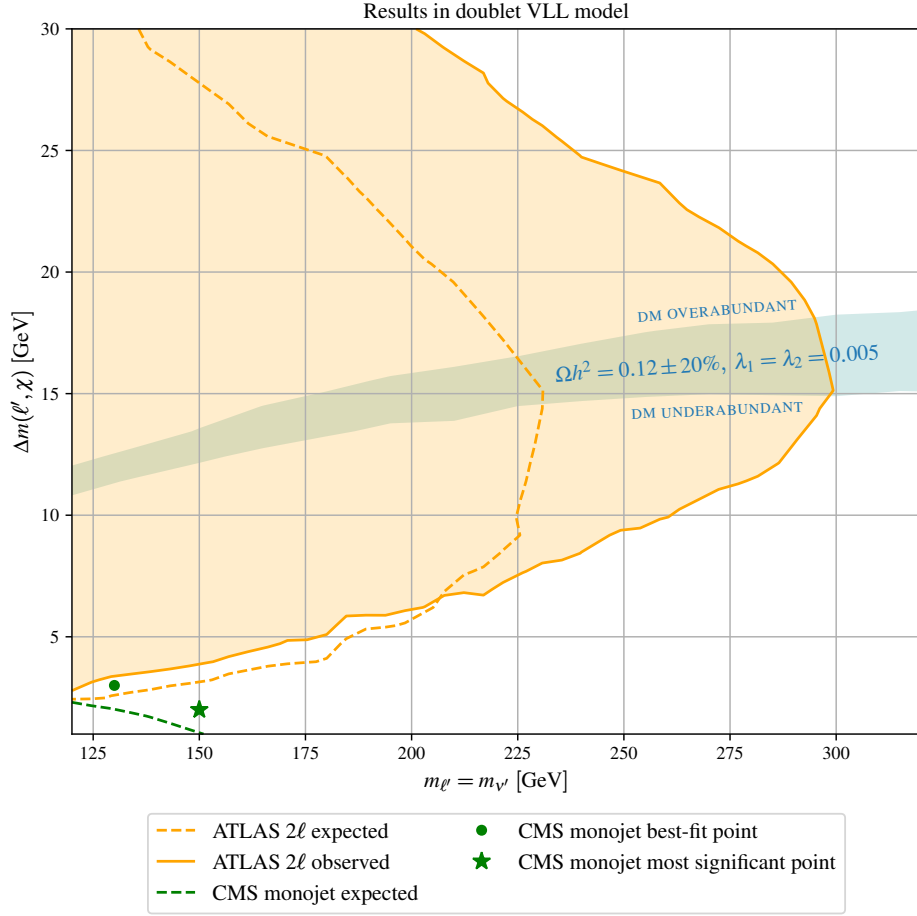


Fig. 15 View of the region of the VLL doublet model parameter space relevant to the LHC excesses. Orange contours show limits from ATLAS-SUSY-2018-16 (2ℓ), while green contour refers to CMS-EXO-20-004 (monojet). Dashed contours indicate expected limits and solid contours denote the edge of the observed excluded regions of the parameter space, shaded correspondingly. Light blue band shows the region approximately featuring a relic abundance Ωh^2 within 20% of the *Planck* measurement. Two interesting non-excluded points are highlighted for the monojet analysis.

Point ($m_{\ell'} = m_{\nu'}, \Delta m(\ell', \chi)$) [GeV]	● CMS monojet best fit (273, 16.3)	★ CMS monojet most significant (284, 20.0)
Significance (p -value)	0.047	0.041
Signal strength $\hat{\mu}$	1.12	1.26

Table 13 Statistics and benchmark information for the significant doublet VLL model points marked in Figure 15.

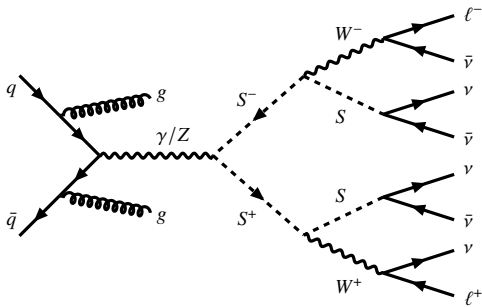


Fig. 16 Soft-lepton signal from pair production of a singly charged scalar S^\pm at LHC, followed by decays to neutral scalars S , themselves decaying invisibly.

they are substantially smaller than the equivalents found for chargino pair production. This is presumably because of the isolation requirements: the processes with $S^{\pm\pm}$ (which have the largest cross sections) contain two off-shell W decays, one of which should be hadronic (so as not to produce same-sign lepton pairs).

The result of these poor efficiencies is a failure of all analyses to constrain the type-II seesaw model in this parameter space. This result is noteworthy by itself since (as mentioned above) this space was previously identified as unconstrained by the LHC. But this situation also makes an exclusion plot impracticable. In lieu of a plot, we provide in Table 14 the results for one point in our scan to which

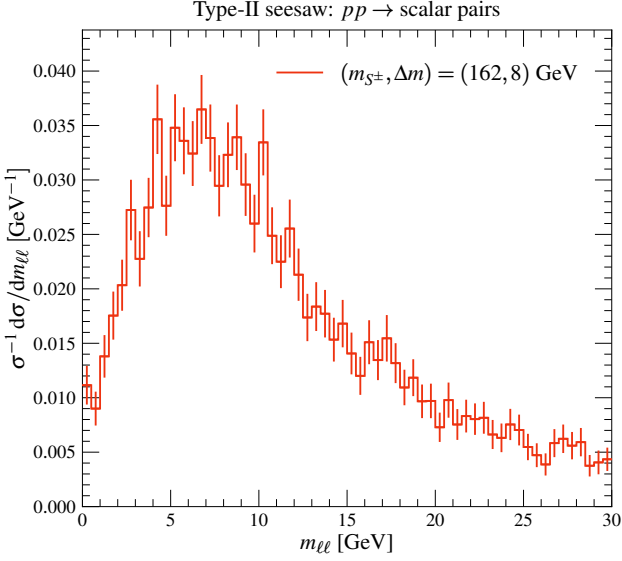


FIG. 17 $m_{\ell\ell}$ distribution for the type-II seesaw model, for $m_{S^\pm} = 162$ GeV. Processes considered are listed in (23) and our simulation relies on matrix elements including up to two additional partons. Here $\Delta m = m_{S^{++}} - m_{S^\pm} = m_{S^\pm} - m_S$.

	CL_s^{exp}	CL_s^{obs}	p -value	$\hat{\mu}$
ATLAS 2ℓ	0.387	0.620	0.050	2.06
ATLAS 3ℓ	0.611	0.615	≥ 0.5	0.62
CMS monojet	0.270	0.395	0.081	1.17
ATLAS monojet	0.553	0.399	0.277	0.72

Table 14 Statistics for the point $(m_{S^\pm}, \Delta m(S^\pm, S)) = (95, 5)$ GeV in the type-II seesaw model. $\text{CL}_s \leq 0.05$ indicates exclusion at 95% CL.

all four analyses¹¹ show at least some sensitivity. This point has $(m_{S^\pm}, \Delta m(S^\pm, S)) = (95, 5)$ GeV and thus corresponds to $\lambda_4 = -0.061$. Table 14 shows that, as for all points in our scan, there is neither an expected nor an observed limit; *i.e.*, all $\text{CL}_s > 0.05$. Nevertheless, the ATLAS 2ℓ and CMS monojet analyses still exhibit excesses visible in the form of expected CL_s values significantly smaller than their observed counterparts. On the other hand, surprisingly, the ATLAS monojet search seems to show the opposite behavior by this metric, though insufficient statistics may be at play here. Meanwhile, while the significance is computed in the usual way for each analysis, we see nothing significant other than $p = 0.050$ for the ATLAS 2ℓ analysis, which is however associated with a signal strength of $\hat{\mu} = 2.06$. Thus even in the best case we can find, this model produces insufficient events passing these analysis selections. By any measure, the type-II seesaw model does not fit the compressed LHC excesses.

¹¹Recall once more that a limit can only be computed based on the most sensitive individual signal region for the ATLAS monojet analysis.

6 Conclusions

We have investigated the compatibility of several supersymmetric and non-supersymmetric models with the soft-lepton and monojet excesses at the LHC, and attempted to connect those excesses with the dark matter relic abundance. The competing models try to explain the excesses through processes with differing topologies, which lead to different distributions of the invariant mass of dileptons, and also to final states with differing average numbers of jets. Taken together, of the cases that we considered, we find that models producing lepton pairs via the decay of a new-physics state through an off-shell Z boson exhibit the best compatibility. The other models that we considered feature decays of new particles via off-shell W bosons or directly to leptons through a two-body process, and both of these cases produce wider distributions of $m_{\ell\ell}$ and possibly events with more jets. This therefore leads to poorer fits of the excesses, and even to cases where the observed limits are stronger than the expected ones. In particular, our results tend to favor the bino-wino MSSM and singlino-higgsino NMSSM explanations for the soft-lepton excesses. But the NMSSM produces not nearly enough monojet events, and we have found that both the doublet vector-like lepton and type-II seesaw models yield even worse fits. This altogether leaves the MSSM as the best option currently on the table. But it too leaves something to be desired.

While we have studied an array of well motivated and (crucially) distinct models, this work is by no means comprehensive. There exist multiple well known BSM scenarios worthy of future examination, including the various N -Higgs-doublet models. Alternatively, some future work on this subject should be aimed at constructing new models optimized from the bottom up to fit these excesses. It would be interesting to consider non-supersymmetric models where decays occur via an off-shell Z boson, or via an off-shell BSM scalar: we are particularly motivated to examine new ways to produce relatively sharply peaked $m_{\ell\ell}$ distributions that are not identical to those seen in this work. We therefore hope to return to these ideas in the near future.

The adaptation of our recasts to MADANALYSIS 5, and a recast of the CMS soft-lepton search [3], are currently ongoing. The latter will allow a comparison of the soft-lepton excesses between the two collaborations, and in particular will help us answer whether the apparent qualitative overlap between ATLAS and CMS soft-lepton excesses is accompanied by compatible signal model fits. At that point, it will also be worthwhile to perform a full statistical combination¹²

¹²We have not done that here for three reasons. (1) We did not want to obscure the fits for the different analyses, especially for points that did not fit well. (2) Without the CMS soft-lepton analysis, we would undersell the total significance. (3) Even using a powerful GPU on a machine with more than 100 GB of RAM, the statistical analysis using PyHF takes $O(5)$ minutes per point; this will only be multiplied in

of the ATLAS soft-lepton, CMS soft-lepton and CMS mono-jet searches using a joint likelihood (since the analyses and signal regions are all independent; but sadly excluding the ATLAS monojet search) in order to obtain the overall best-fit points to all the different excesses and provide potentially provocative discovery p -values for excluding the Standard Model.

Acknowledgements B. F., M. D. G., and T. M. are supported in part by Grant ANR-21-CE31-0013, Project DMwithLLPatLHC, from the *Agence Nationale de la Recherche* (ANR), France. We thank Jack Y. Araz for correspondence about `SPEY`.

Appendix A: Selections and yields for the inclusive off-shell WZ selection

This appendix (starting on the next page) contains the definitions of the inclusive signal regions for the 3ℓ analysis, ATLAS-SUSY-2019-09, and the yields and discovery p -values for each inclusive signal region.

complexity for the combination, and for technical reasons that machine could not run `SPEY` due to the too recent `python` version running on it.

incSR ^{offWZ} _{highE_t} -nj					
	a	b	c1	c2	
$m_{\ell\ell}^{\text{min}}$ [GeV]	[1, 12] SR ^{offWZ} _{highE_t} -nj [a]	[12, 15] SR ^{offWZ} _{highE_t} -nj [b]	[1, 20] SR ^{offWZ} _{highE_t} -nj [a-c]	[15, 20] SR ^{offWZ} _{highE_t} -nj [c]	
incSR ^{offWZ} _{lowE_t}					
	b	c	b	c	
$m_{\ell\ell}^{\text{min}}$ [GeV]	[12, 15] SR ^{offWZ} _{lowE_t} -0j [b], SR ^{offWZ} _{lowE_t} -nj [b]	[12, 20] SR ^{offWZ} _{lowE_t} -0j [b-c], SR ^{offWZ} _{lowE_t} -nj [b-c]	[12, 15] SR ^{offWZ} _{highE_t} -0j [b], SR ^{offWZ} _{highE_t} -nj [b]	[12, 20] SR ^{offWZ} _{highE_t} -0j [b-c], SR ^{offWZ} _{highE_t} -nj [b-c]	
incSR ^{offWZ}					
	d	e1	e2	f1	f2
$m_{\ell\ell}^{\text{min}}$ [GeV]	[12, 30] SR ^{offWZ} _{lowE_t} -0j [b-d], SR ^{offWZ} _{lowE_t} -nj [b-d], SR ^{offWZ} _{highE_t} -0j [b-d], SR ^{offWZ} _{highE_t} -nj [b-d]	[12, 40] SR ^{offWZ} _{lowE_t} -0j [b-e], SR ^{offWZ} _{lowE_t} -nj [b-e], SR ^{offWZ} _{highE_t} -0j [b-e], SR ^{offWZ} _{highE_t} -nj [b-e]	[20, 40] SR ^{offWZ} _{lowE_t} -0j [c-e], SR ^{offWZ} _{lowE_t} -nj [c-e], SR ^{offWZ} _{highE_t} -0j [c-e], SR ^{offWZ} _{highE_t} -nj [c-e]	[12, 60] SR ^{offWZ} _{lowE_t} -0j [c-f2], SR ^{offWZ} _{lowE_t} -nj [c-f2], SR ^{offWZ} _{highE_t} -0j [c-f2], SR ^{offWZ} _{highE_t} -nj [c-f]	[30, 60] SR ^{offWZ} _{lowE_t} -0j [e-f2], SR ^{offWZ} _{lowE_t} -nj [e-f2], SR ^{offWZ} _{highE_t} -0j [e-f2], SR ^{offWZ} _{highE_t} -nj [e-f]
incSR ^{offWZ}					
	g1	g2	g3	g4	
$m_{\ell\ell}^{\text{min}}$ [GeV]	[12, 75] SR ^{offWZ} _{lowE_t} -0j [b-g2], SR ^{offWZ} _{lowE_t} -nj [b-g2], SR ^{offWZ} _{highE_t} -0j [b-g2], SR ^{offWZ} _{highE_t} -nj [b-g]	[30, 75] SR ^{offWZ} _{lowE_t} -0j [e-g2], SR ^{offWZ} _{lowE_t} -nj [e-g2], SR ^{offWZ} _{highE_t} -0j [e-g2], SR ^{offWZ} _{highE_t} -nj [e-g]	[40, 75] SR ^{offWZ} _{lowE_t} -0j [f1-g2], SR ^{offWZ} _{lowE_t} -nj [f1-g2], SR ^{offWZ} _{highE_t} -0j [f1-g2], SR ^{offWZ} _{highE_t} -nj [f1-g]	[60, 75] SR ^{offWZ} _{lowE_t} -0j [g1-g2], SR ^{offWZ} _{lowE_t} -nj [g1-g2], SR ^{offWZ} _{highE_t} -0j [g1-g2], SR ^{offWZ} _{highE_t} -nj [g]	

Table 15 Summary of the selection criteria defining the inclusive SRs in the off-shell WZ selection.

SR	N_{obs}	N_{exp}	$p(s=0)$
$\text{incSR}_{\text{high}E_t}^{\text{offWZ}} - \text{nja}$	3	6.0 ± 1.6	0.50
$\text{incSR}_{\text{high}E_t}^{\text{offWZ}} - \text{njb}$	2	1.4 ± 0.6	0.30
$\text{incSR}_{\text{high}E_t}^{\text{offWZ}} - \text{njc1}$	7	9.5 ± 2.2	0.50
$\text{incSR}_{\text{high}E_t}^{\text{offWZ}} - \text{njc2}$	2	2.1 ± 0.8	0.50
$\text{incSR}_{\text{low}E_t}^{\text{offWZ}} - \text{b}$	31	36 ± 4	0.50
$\text{incSR}_{\text{high}E_t}^{\text{offWZ}} - \text{b}$	3	3.0 ± 0.9	0.50
$\text{incSR}_{\text{low}E_t}^{\text{offWZ}} - \text{c}$	86	88 ± 7	0.50
$\text{incSR}_{\text{high}E_t}^{\text{offWZ}} - \text{c}$	9	9.3 ± 1.5	0.50
$\text{incSR}_{\text{low}E_t}^{\text{offWZ}} - \text{d}$	202	184 ± 12	0.16
$\text{incSR}_{\text{high}E_t}^{\text{offWZ}} - \text{e1}$	332	308 ± 17	0.16
$\text{incSR}_{\text{high}E_t}^{\text{offWZ}} - \text{e2}$	298	269 ± 15	0.10
$\text{incSR}_{\text{high}E_t}^{\text{offWZ}} - \text{f1}$	479	457 ± 22	0.23
$\text{incSR}_{\text{high}E_t}^{\text{offWZ}} - \text{f2}$	277	272 ± 13	0.37
$\text{incSR}_{\text{low}E_t}^{\text{offWZ}} - \text{g1}$	620	593 ± 28	0.21
$\text{incSR}_{\text{high}E_t}^{\text{offWZ}} - \text{g2}$	418	408 ± 20	0.32
$\text{incSR}_{\text{high}E_t}^{\text{offWZ}} - \text{g3}$	288	285 ± 16	0.38
$\text{incSR}_{\text{high}E_t}^{\text{offWZ}} - \text{g4}$	141	136 ± 10	0.35

Table 16 Observed (N_{obs}) yields after the discovery fit and expected (N_{exp}) after the background-only fit, for the inclusive SRs of the off-shell WZ selection. The last column indicates the discovery p -value ($p(s=0)$). If the observed yield is below the expected yield, the p -value is capped at 0.5.

References

1. ATLAS collaboration, *Searches for electroweak production of supersymmetric particles with compressed mass spectra in $\sqrt{s} = 13$ TeV pp collisions with the ATLAS detector*, *Phys. Rev. D* **101** (2020) 052005 [[1911.12606](#)].
2. ATLAS collaboration, *Search for chargino–neutralino pair production in final states with three leptons and missing transverse momentum in $\sqrt{s} = 13$ TeV pp collisions with the ATLAS detector*, *Eur. Phys. J. C* **81** (2021) 1118 [[2106.01676](#)].
3. CMS collaboration, *Search for supersymmetry in final states with two or three soft leptons and missing transverse momentum in proton-proton collisions at $\sqrt{s} = 13$ TeV*, *J. High Energy Phys.* **04** (2022) 091 [[2111.06296](#)].
4. A. Canepa, T. Han and X. Wang, *The Search for Electroweakinos*, *Ann. Rev. Nucl. Part. Sci.* **70** (2020) 425 [[2003.05450](#)].
5. T. Buanes, I.n. Lara, K. Rolbiecki and K. Sakurai, *LHC constraints on electroweakino dark matter revisited*, *Phys. Rev. D* **107** (2023) 095021 [[2208.04342](#)].
6. J. Cao, F. Li, J. Lian, Y. Pan and D. Zhang, *Impact of LHC probes of SUSY and recent measurement of $(g - 2)_\mu$ on \mathbb{Z}_3 -NMSSM*, *Sci. China Phys. Mech. Astron.* **65** (2022) 291012 [[2204.04710](#)].
7. F. Domingo, U. Ellwanger and C. Hugonie, *M_W , dark matter and a_μ in the NMSSM*, *Eur. Phys. J. C* **82** (2022) 1074 [[2209.03863](#)].
8. R.K. Barman, G. Bélanger, B. Bhattacharjee, R.M. Godbole and R. Sengupta, *Is Light Neutralino Thermal Dark Matter in the Phenomenological Minimal Supersymmetric Standard Model Ruled Out?*, *Phys. Rev. Lett.* **131** (2023) 011802 [[2207.06238](#)].
9. S. Baum, M. Carena, T. Ou, D. Rocha, N.R. Shah and C.E.M. Wagner, *Lighting up the LHC with Dark Matter*, *J. High Energy Phys.* **11** (2023) 037 [[2303.01523](#)].
10. G. Stark, C.A. Ots and M. Hance, *Reduce, Reuse, Reinterpret: an end-to-end pipeline for recycling particle physics results*, [2306.11055](#).
11. H. Baer, V. Barger, X. Tata and K. Zhang, *Winos from natural SUSY at the high luminosity LHC*, *Phys. Rev. D* **109** (2024) 015027 [[2310.10829](#)].
12. J. Cao, L. Meng and Y. Yue, *Electron and muon anomalous magnetic moments in the \mathbb{Z}_3 -NMSSM*, *Phys. Rev. D* **108** (2023) 035043 [[2306.06854](#)].
13. S. Ashanujjaman and S.P. Maharathy, *Probing compressed mass spectra in the type-II seesaw model at the LHC*, *Phys. Rev. D* **107** (2023) 115026 [[2305.06889](#)].
14. L.M. Carpenter, H. Gilmer, J. Kawamura and T. Murphy, *Taking aim at the wino-Higgsino plane with the LHC*, *Phys. Rev. D* **109** (2024) 015012 [[2309.07213](#)].
15. H. Baer, V. Barger, J. Bolich, J. Dutta and D. Sengupta, *Natural anomaly mediation from the landscape with implications for LHC SUSY searches*, *Phys. Rev. D* **109** (2024) 035011 [[2311.18120](#)].
16. S. Roy and C.E.M. Wagner, *Dark Matter searches with photons at the LHC*, [2401.08917](#).
17. H. Baer, V. Barger, D. Martinez and S. Salam, *Weak Scale Supersymmetry Emergent from the String Landscape*, *Entropy* **26** (2024) 275 [[2402.17859](#)].
18. M. Chakraborti, S. Heinemeyer and I. Saha, *Consistent Excesses in the Search for $\tilde{\chi}_2^0 \tilde{\chi}_1^\pm$: Wino/bino vs. Higgsino Dark Matter*, [2403.14759](#).
19. S.P. Martin, *Implications of purity constraints on light higgsinos*, [2403.19598](#).
20. D. Agin, B. Fuks, M.D. Goodsell and T. Murphy, *Monojets reveal overlapping excesses for light compressed higgsinos*, [2311.17149](#).
21. ATLAS collaboration, *Search for new phenomena in events with an energetic jet and missing transverse momentum in pp collisions at $\sqrt{s} = 13$ TeV with the ATLAS detector*, *Phys. Rev. D* **103** (2021) 112006 [[2102.10874](#)].
22. CMS collaboration, *Search for new particles in events with energetic jets and large missing transverse momentum in proton-proton collisions at $\sqrt{s} = 13$ TeV*, *J. High Energy Phys.* **11** (2021) 153 [[2107.13021](#)].
23. H. Baer, V. Barger and A. Mustafayev, *Implications of a 125 GeV Higgs scalar for LHC SUSY and neutralino dark matter searches*, *Phys. Rev. D* **85** (2012) 075010 [[1112.3017](#)].
24. M. Chakraborti, U. Chattopadhyay and S. Poddar, *How light a higgsino or a wino dark matter can become in a compressed scenario of MSSM*, *J. High Energy Phys.* **09** (2017) 064 [[1702.03954](#)].
25. ATLAS collaboration, “ATLAS Run 2 searches for electroweak production of supersymmetric particles interpreted within the pMSSM.” February, 2024.
26. M.D. Goodsell, *HackAnalysis 2: A powerful and hackable recasting tool*, [2406.10042](#).
27. P. Jackson and C. Rogan, *Recursive Jigsaw Reconstruction: HEP event analysis in the presence of kinematic and combinatoric ambiguities*, *Phys. Rev. D* **96** (2017) 112007 [[1705.10733](#)].
28. S. Montesano, *Ricerca di particelle supersimmetriche nell’ambito dell’esperimento ATLAS*, Master’s thesis, Milano, Università degli Studi di Milano, 2005.
29. U. De Sanctis, T. Lari, S. Montesano and C. Troncon, *Perspectives for the detection and measurement of Supersymmetry in the focus point region of mSUGRA*

- models with the ATLAS detector at LHC, *Eur. Phys. J. C* **52** (2007) 743 [0704.2515].
30. The ATLAS Collaboration, *SimpleAnalysis: Truth-level Analysis Framework*, ATL-PHYS-PUB-2022-017.
 31. L. Heinrich, M. Feickert, G. Stark and K. Cranmer, *pyhf: pure-Python implementation of HistFactory statistical models*, *J. Open Source Softw.* **6** (2021) 2823.
 32. M. Drees, H. Dreiner, D. Schmeier, J. Tattersall and J.S. Kim, *CheckMATE: Confronting your Favourite New Physics Model with LHC Data*, *Comput. Phys. Commun.* **187** (2015) 227 [1312.2591].
 33. D. Dercks, N. Desai, J.S. Kim, K. Rolbiecki, J. Tattersall and T. Weber, *CheckMATE 2: From the model to the limit*, *Comput. Phys. Commun.* **221** (2017) 383 [1611.09856].
 34. C. Rogan, *Restframes*, <http://restframes.com/>.
 35. R. Brun and F. Rademakers, *ROOT: An object oriented data analysis framework*, *Nucl. Instrum. Meth. A* **389** (1997) 81.
 36. GAMBIT collaboration, *GAMBIT: The Global and Modular Beyond-the-Standard-Model Inference Tool*, *Eur. Phys. J. C* **77** (2017) 784 [1705.07908].
 37. E. Conte, B. Fuks and G. Serret, *MadAnalysis 5, A User-Friendly Framework for Collider Phenomenology*, *Comput. Phys. Commun.* **184** (2013) 222 [1206.1599].
 38. E. Conte, B. Dumont, B. Fuks and C. Wymant, *Designing and recasting LHC analyses with MadAnalysis 5*, *Eur. Phys. J. C* **74** (2014) 3103 [1405.3982].
 39. E. Conte and B. Fuks, *Confronting new physics theories to LHC data with MADANALYSIS 5*, *Int. J. Mod. Phys. A* **33** (2018) 1830027 [1808.00480].
 40. J.A. Nelder and R. Mead, *A Simplex Method for Function Minimization*, *Comput. J.* **7** (1965) 308.
 41. P. Artoisenet, R. Frederix, O. Mattelaer and R. Rietkerk, *Automatic spin-entangled decays of heavy resonances in Monte Carlo simulations*, *J. High Energy Phys.* **03** (2013) 015 [1212.3460].
 42. J. Alwall, C. Duhr, B. Fuks, O. Mattelaer, D.G. Öztürk and C.-H. Shen, *Computing decay rates for new physics theories with FeynRules and MadGraph5_aMC@NLO*, *Comput. Phys. Commun.* **197** (2015) 312 [1402.1178].
 43. J. Alwall, R. Frederix, S. Frixione, V. Hirschi, F. Maltoni, O. Mattelaer et al., *The automated computation of tree-level and next-to-leading order differential cross sections, and their matching to parton shower simulations*, *J. High Energy Phys.* **07** (2014) 079 [1405.0301].
 44. C. Bierlich et al., *A comprehensive guide to the physics and usage of PYTHIA 8.3*, *SciPost Phys. Codeb.* **2022** (2022) 8 [2203.11601].
 45. M.L. Mangano, M. Moretti, F. Piccinini and M. Treccani, *Matching matrix elements and shower evolution for top-quark production in hadronic collisions*, *J. High Energy Phys.* **01** (2007) 013 [hep-ph/0611129].
 46. J. Alwall, S. de Visscher and F. Maltoni, *QCD radiation in the production of heavy colored particles at the LHC*, *J. High Energy Phys.* **02** (2009) 017 [0810.5350].
 47. M.D. Goodsell and A. Joury, *BSMART: Simple and fast parameter space scans*, *Comput. Phys. Commun.* **297** (2024) 109057 [2301.01154].
 48. C. Degrande, C. Duhr, B. Fuks, D. Grellscheid, O. Mattelaer and T. Reiter, *UFO - The Universal FeynRules Output*, *Comput. Phys. Commun.* **183** (2012) 1201 [1108.2040].
 49. L. Darmé et al., *UFO 2.0: the 'Universal Feynman Output' format*, *Eur. Phys. J. C* **83** (2023) 631 [2304.09883].
 50. C. Duhr and B. Fuks, *A superspace module for the FeynRules package*, *Comput. Phys. Commun.* **182** (2011) 2404 [1102.4191].
 51. R.D. Ball et al., *Parton distributions with LHC data*, *Nucl. Phys. B* **867** (2013) 244 [1207.1303].
 52. A. Buckley, J. Ferrando, S. Lloyd, K. Nordström, B. Page, M. Rüfenacht et al., *LHAPDF6: parton density access in the LHC precision era*, *Eur. Phys. J. C* **75** (2015) 132 [1412.7420].
 53. J. Alwall et al., *A Standard format for Les Houches event files*, *Comput. Phys. Commun.* **176** (2007) 300 [hep-ph/0609017].
 54. A. Buckley, M. Filipovich, C. Gutsche, N. Rozinsky, S. Thor, Y. Yeh et al., *Consistent, multidimensional differential histogramming and summary statistics with YODA 2*, **2312.15070**.
 55. B. Fuks, M. Klasen, D.R. Lamprea and M. Rothering, *Precision predictions for electroweak superpartner production at hadron colliders with RESUMMINO*, *Eur. Phys. J. C* **73** (2013) 2480 [1304.0790].
 56. J. Fiaschi, B. Fuks, M. Klasen and A. Neuwirth, *Electroweak superpartner production at 13.6 TeV with Resummino*, *Eur. Phys. J. C* **83** (2023) 707 [2304.11915].
 57. ATLAS collaboration, *Object-based missing transverse momentum significance in the ATLAS detector*, ATL-CONF-2018-038.
 58. C.G. Lester and D.J. Summers, *Measuring masses of semiinvisibly decaying particles pair produced at hadron colliders*, *Phys. Lett. B* **463** (1999) 99 [hep-ph/9906349].

59. H.-C. Cheng and Z. Han, *Minimal Kinematic Constraints and $m(T_2)$* , *J. High Energy Phys.* **12** (2008) 063 [[0810.5178](#)].
60. ATLAS collaboration, *Performance of electron and photon triggers in ATLAS during LHC Run 2*, *Eur. Phys. J. C* **80** (2020) 47 [[1909.00761](#)].
61. ATLAS collaboration, *Performance of the ATLAS muon triggers in Run 2*, *JINST* **15** (2020) P09015 [[2004.13447](#)].
62. A. Albert, *Implementation of a search for new phenomena in events featuring energetic jets and missing transverse energy (137 fb⁻¹; 13 TeV; CMS-EXO-20-004)*, [10.14428/DVN/IRF7ZL](#) (2021).
63. D. Agin, *Implementation of a search for new physics with jets and missing transverse energy (139 fb⁻¹; 13 TeV; ATLAS-EXOT-2018-06)*, [10.14428/DVN/REPAMM](#) (2023).
64. DELPHES 3 collaboration, *DELPHES 3, A modular framework for fast simulation of a generic collider experiment*, *J. High Energy Phys.* **02** (2014) 057 [[1307.6346](#)].
65. J.F. Gunion and H.E. Haber, *Two-body decays of neutralinos and charginos*, *Phys. Rev. D* **37** (1988) 2515.
66. PLANCK collaboration, *Planck 2018 results. VI. Cosmological parameters*, *Astron. Astrophys.* **641** (2020) A6 [[1807.06209](#)].
67. F. Staub, *SARAH*, [0806.0538](#).
68. F. Staub, *SARAH 4 : A tool for (not only SUSY) model builders*, *Comput. Phys. Commun.* **185** (2014) 1773 [[1309.7223](#)].
69. M.D. Goodsell, K. Nickel and F. Staub, *Two-Loop Higgs mass calculations in supersymmetric models beyond the MSSM with SARAH and SPheno*, *Eur. Phys. J. C* **75** (2015) 32 [[1411.0675](#)].
70. M.D. Goodsell, S. Liebler and F. Staub, *Generic calculation of two-body partial decay widths at the full one-loop level*, *Eur. Phys. J. C* **77** (2017) 758 [[1703.09237](#)].
71. W. Porod, *SPheno, a program for calculating supersymmetric spectra, SUSY particle decays and SUSY particle production at e⁺ e⁻ colliders*, *Comput. Phys. Commun.* **153** (2003) 275 [[hep-ph/0301101](#)].
72. W. Porod and F. Staub, *SPheno 3.1: Extensions including flavour, CP-phases and models beyond the MSSM*, *Comput. Phys. Commun.* **183** (2012) 2458 [[1104.1573](#)].
73. M.D. Goodsell, K. Nickel and F. Staub, *Two-loop corrections to the Higgs masses in the NMSSM*, *Phys. Rev. D* **91** (2015) 035021 [[1411.4665](#)].
74. M. Goodsell, K. Nickel and F. Staub, *Generic two-loop Higgs mass calculation from a diagrammatic approach*, *Eur. Phys. J. C* **75** (2015) 290 [[1503.03098](#)].
75. J. Braathen, M.D. Goodsell and F. Staub, *Supersymmetric and non-supersymmetric models without catastrophic Goldstone bosons*, *Eur. Phys. J. C* **77** (2017) 757 [[1706.05372](#)].
76. G. Belanger, F. Boudjema, A. Pukhov and A. Semenov, *micrOMEGAs: A Tool for dark matter studies*, *Nuovo Cim. C* **033N2** (2010) 111 [[1005.4133](#)].
77. G. Belanger, F. Boudjema, A. Pukhov and A. Semenov, *micrOMEGAs_3: A program for calculating dark matter observables*, *Comput. Phys. Commun.* **185** (2014) 960 [[1305.0237](#)].
78. G. Alguero, G. Belanger, F. Boudjema, S. Chakraborti, A. Goudelis, S. Kraml et al., *micrOMEGAs 6.0: N-component dark matter*, *Comput. Phys. Commun.* **299** (2024) 109133 [[2312.14894](#)].
79. A. Belyaev, N.D. Christensen and A. Pukhov, *CalcHEP 3.4 for collider physics within and beyond the Standard Model*, *Comput. Phys. Commun.* **184** (2013) 1729 [[1207.6082](#)].
80. H. Bahl, T. Biekötter, S. Heinemeyer, C. Li, S. Paasch, G. Weiglein et al., *HiggsTools: BSM scalar phenomenology with new versions of HiggsBounds and HiggsSignals*, *Comput. Phys. Commun.* **291** (2023) 108803 [[2210.09332](#)].
81. SModelS collaboration, *SModelS: A Tool for Making Systematic Use of Simplified Models Results*, *J. Phys. Conf. Ser.* **762** (2016) 012076.
82. G. Alguero, J. Heisig, C.K. Khosa, S. Kraml, S. Kulkarni, A. Lessa et al., *Constraining new physics with SModelS version 2*, *J. High Energy Phys.* **08** (2022) 068 [[2112.00769](#)].
83. M. Mahdi Altakach, S. Kraml, A. Lessa, S. Narasimha, T. Pascal and W. Waltenberger, *SModelS v2.3: enabling global likelihood analyses*, *SciPost Phys.* **15** (2023) 185 [[2306.17676](#)].
84. J.Y. Araz, *Spey: Smooth inference for reinterpretation studies*, *SciPost Phys.* **16** (2024) 032 [[2307.06996](#)].
85. A.L. Read, *Presentation of search results: The CL_s technique*, *J. Phys. G* **28** (2002) 2693.
86. U. Ellwanger, C. Hugonie and A.M. Teixeira, *The Next-to-Minimal Supersymmetric Standard Model*, *Phys. Rept.* **496** (2010) 1 [[0910.1785](#)].
87. J.E. Kim and H.P. Nilles, *The μ Problem and the Strong CP Problem*, *Phys. Lett. B* **138** (1984) 150.
88. Y. Bai and J. Berger, *Lepton Portal Dark Matter*, *J. High Energy Phys.* **08** (2014) 153 [[1402.6696](#)].
89. W. Konetschny and W. Kummer, *Nonconservation of Total Lepton Number with Scalar Bosons*, *Phys. Lett. B* **70** (1977) 433.

90. T.P. Cheng and L.-F. Li, *Neutrino Masses, Mixings and Oscillations in $SU(2) \times U(1)$ Models of Electroweak Interactions*, *Phys. Rev. D* **22** (1980) 2860.
91. G. Lazarides, Q. Shafi and C. Wetterich, *Proton Lifetime and Fermion Masses in an $SO(10)$ Model*, *Nucl. Phys. B* **181** (1981) 287.
92. J. Schechter and J.W.F. Valle, *Neutrino masses in $SU(2) \otimes U(1)$ theories*, *Phys. Rev. D* **22** (1980) 2227.
93. R.N. Mohapatra and G. Senjanovic, *Neutrino Masses and Mixings in Gauge Models with Spontaneous Parity Violation*, *Phys. Rev. D* **23** (1981) 165.
94. Y. Cai, T. Han, T. Li and R. Ruiz, *Lepton Number Violation: Seesaw Models and Their Collider Tests*, *Front. in Phys.* **6** (2018) 40 [[1711.02180](#)].
95. S. Iguro, S. Okawa and Y. Omura, *Light lepton portal dark matter meets the LHC*, *J. High Energy Phys.* **03** (2023) 010 [[2208.05487](#)].
96. N.D. Christensen, P. de Aquino, C. Degrande, C. Duhr, B. Fuks, M. Herquet et al., *A Comprehensive approach to new physics simulations*, *Eur. Phys. J. C* **71** (2011) 1541 [[0906.2474](#)].
97. A. Alloul, N.D. Christensen, C. Degrande, C. Duhr and B. Fuks, *FeynRules 2.0 - A complete toolbox for tree-level phenomenology*, *Comput. Phys. Commun.* **185** (2014) 2250 [[1310.1921](#)].
98. M. Backovic, K. Kong and M. McCaskey, *MadDM v.1.0: Computation of Dark Matter Relic Abundance Using MadGraph5*, *Physics of the Dark Universe* **5-6** (2014) 18 [[1308.4955](#)].
99. F. Ambrogio, C. Arina, M. Backovic, J. Heisig, F. Maltoni, L. Mantani et al., *MadDM v.3.0: a Comprehensive Tool for Dark Matter Studies*, *Phys. Dark Univ.* **24** (2019) 100249 [[1804.00044](#)].
100. C. Arina, J. Heisig, F. Maltoni, D. Massaro and O. Mattelaer, *Indirect dark-matter detection with MadDM v3.2 – Lines and Loops*, *Eur. Phys. J. C* **83** (2023) 241 [[2107.04598](#)].
101. T. Toma, *Internal Bremsstrahlung Signature of Real Scalar Dark Matter and Consistency with Thermal Relic Density*, *Phys. Rev. Lett.* **111** (2013) 091301 [[1307.6181](#)].
102. F. Giacchino, L. Lopez-Honorez and M.H.G. Tytgat, *Scalar Dark Matter Models with Significant Internal Bremsstrahlung*, *JCAP* **10** (2013) 025 [[1307.6480](#)].
103. S. Weinberg, *Baryon- and lepton-nonconserving processes*, *Phys. Rev. Lett.* **43** (1979) 1566.
104. S. Ashanujjaman, K. Ghosh and K. Huitu, *Type II seesaw model: Searching for the LHC-elusive low-mass triplet Higgs bosons at e^-e^+ colliders*, *Phys. Rev. D* **106** (2022) 075028.
105. B. Fuks, M. Nemevšek and R. Ruiz, *Doubly Charged Higgs Boson Production at Hadron Colliders*, *Phys. Rev. D* **101** (2020) 075022 [[1912.08975](#)].